

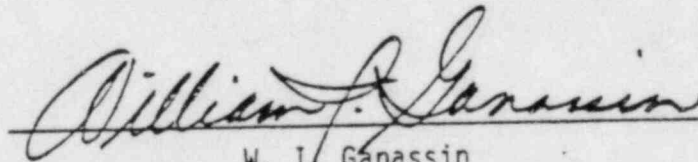
SRO-316
August 1982

STRUCTURAL REVIEW OF THE
CONNECTICUT YANKEE NUCLEAR GENERATING PLANT,
CONTAINMENT STRUCTURE UNDER COMBINED LOADS

By

C. Y. Liaw
EGG/SRO

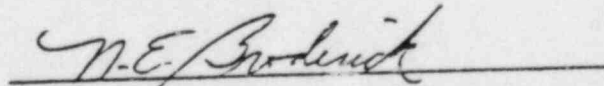
N. C. Tsai and S. Pazargadi
NCT Engineering, Inc.



W. I. Ganassin
Mechanical Engineering, Department Manager

This document is UNCLASSIFIED.

Derivative
Classifier:



N. E. Broderick
Department Manager

XA Copy Has Been Sent to PDR

8209030274 XA

ABSTRACT

A structural reassessment of the containment structure of the Connecticut Yankee Nuclear Generating Plant at Haddam Neck, Connecticut was performed for the Nuclear Regulatory Commission (NRC) as part of the Systematic Evaluation Program. Conclusions about the ability of the containment structure to withstand the abnormal/extreme environment are presented.

The reassessment focused mainly on the overall structural integrity of the containment building for the abnormal/extreme environment. In this case, the abnormal-environmental condition is caused by a loss-of-coolant accident (LOCA). The extreme environment condition is the safe-shutdown earthquake (SSE). Seismic loads of the SSE are based on the site-specific ground-response spectra developed by Lawrence Livermore National Laboratory for the Haddam Neck site. Thermal and pressure loads of the LOCA are developed from pressure and temperature profiles for the LOCA conditions provided by NRC.

FOREWORD

The U.S. Nuclear Regulatory Commission (NRC) is conducting the Systematic Evaluation Program (SEP). The Program is a plant-by-plant reassessment of the safety of eleven operating nuclear reactors that received construction permits between 1956 and 1967. Many safety criteria have changed since these plants were licensed. The purpose of the SEP is to develop a current, documented basis for the safety of older facilities.

For the Connecticut Yankee Plant, the containment structure was selected for evaluation of the abnormal extreme environment case. In this case, the abnormal-environmental condition is caused by a loss-of-coolant accident (LOCA). The extreme environment condition is the safe-shutdown earthquake (SSE).

This report reflects a collective effort on the part of the following people:

Lo, T., and Nelson, T. A., [Lawrence Livermore National Laboratory (LLNL)], who provided project management support and reviewed the report.

Liaw, C. Y., (EG&G/San Ramon Operations), who conducted the structural reevaluation of the concrete containment structure.

Tsai, N. C. (NCT Engineering, Inc.), who conducted the structural reevaluation of the steel liner plate system.

The authors wish to thank P. Y. Chen and S. Brown, technical monitors of this work at the Office of Nuclear Reactor Regulation (NRR), for their continuing support.

CONTENTS

	<u>Page</u>
1. INTRODUCTION.	1-1
1.1 Scope of Work	1-1
1.2 Structure Description.	1-1
1.3 Loads and Load Combintions	1-4
1.4 Material Properties	1-8
2. ANALYSIS OF CONTAINMENT SHELL STRUCTURE.	2-1
2.1 Analytical Model	2-1
2.2 Method of Analysis.	2-2
2.3 Results of Analysis	2-4
3. ANALYSIS OF THE LINER SYSTEM	3-1
3.1 Assumptions	3-1
3.2 Initial Membrane Loads in Liner Plate	3-2
3.3 Analysis Models and Unbalanced Forces	3-6
3.3.1 Case 1 - Meridional Strip of Flat Linear Across the Insulation	3-6
3.3.2 Case 2 - Circumferential Liner Strip with One Bent Plate	3-9
3.4 Analysis and Results	3-11
4. SUMMARY AND CONCLUSION	4-1
4.1 Concrete Shell Structure.	4-1
4.2 Liner-Plate System.	4-2
APPENDIX A DERIVATION OF FLAT-PLATE STIFFNESS K_{FP}	A-1
APPENDIX B DERIVATION OF EQUIVALENT SPRING K'	B-1
APPENDIX C DERIVATION OF POST YIELD IN-PLANE STIFFNESS, K_{BP} , OF A BENT PLATE.	C-1

ILLUSTRATIONS

<u>Figure</u>		<u>Page</u>
1	Reactor containment building	1-2
2	Containment pressure the temperature response for the loss-of-coolant accident (LOCA)	1-5
3	Accident temperature gradients through the uninsulated containment wall and dome	1-6
4	Calculated responses due to dead load	2-5
5	Antisymmetrical mode shapes	2-6
6	Symmetrical mode shapes.	2-7
7	Calculated responses due to horizontal component of SSE	2-8
8	Calculated responses due to vertical component of SSE.	2-9
9	Calculated responses due to SSE	2-10
10	Calculated responses due to pressure load (39.3 psig).	2-11
11	Calculated responses due to thermal load of Case 1.	2-12
12	Calculated responses due to thermal load of Case 2.	2-13
13	Calculated responses due to thermal load of Case 3.	2-14
14	Analysis Case 1 - a meridional strip of flat linear system	3-3
15	Analysis Case 2 - a circumferential liner strip with a bent plate.	3-4
16	Analysis model for Case 1	3-7
17	In-plane stiffness for flat plate	3-8
18	Lateral stiffness K_C for a stud in the concrete.	3-8
19	Analysis model for Case 2	3-10
20	In-plane stiffness of bent plate, K_{BP} in the post- yield condition	3-12
A.1	Model for determining in-plane stiffness K_{FP} for a flat plate	A-2
A.2	Approximate analysis model for determining deflection y_a	A-2
A.3	Analysis model for determining deflection y_b	A-2
B.1	Equivalent spring for spring series.	B-3
C.1	A bent plate subjected to axial load	C-2
C.2	Force vs. transverse deflection relationship for an axially-loaded bent plate	C-3
C.3	Force vs. axial displacement relationship.	C-3

TABLES

<u>Table</u>		<u>Page</u>
1	Site specific spectrum	1-7
2	Material properties	1-8
3	Selected cases for LOCA.	2-3
4	Forces and moments in concrete shell	3-13
5	Liner membrane strains	3-14
6	Liner membrane force and unbalanced force in Case 1 analysis model.	3-14
7	Summary of analysis results and ASME allowables.	3-14

1. INTRODUCTION

1.1 SCOPE OF WORK

Structural reassessment of nuclear power plants is one facet of the Systematic Evaluation Program (SEP) conducted by the Nuclear Regulatory Commission (NRC). This report is a structural review of the containment building of the Connecticut Yankee Nuclear Power Plant. We evaluated the overall structural integrity of the containment building for the abnormal/extreme environmental condition as defined in the ASME Boiler and Pressure Vessel Code, Section III (ASME code). In this instance, the abnormal-environment case is that induced by a LOCA, and the extreme-environment case is induced by the SSE.

Our reassessment combined the accident and seismic event with existing load conditions on the containment building. We then evaluated the containment building's and its steel liner's ability to withstand the abnormal/extreme-environment condition. Because the primary purpose of this analysis is to evaluate the overall structural integrity of the containment building, local load effects are not considered.

1.2 STRUCTURE DESCRIPTION

The reactor containment building of the Connecticut Yankee plant houses the nuclear steam supply system. This building is a vertical, cylindrical, reinforced concrete structure (Figure 1). The inside diameter is 135 ft; the inside height is 189 ft. The containment walls are 4.5 ft thick, the dome is 2.5 ft thick, and the base slab is about 9 ft thick. The dome has an inside radius of 67 ft 6 in.

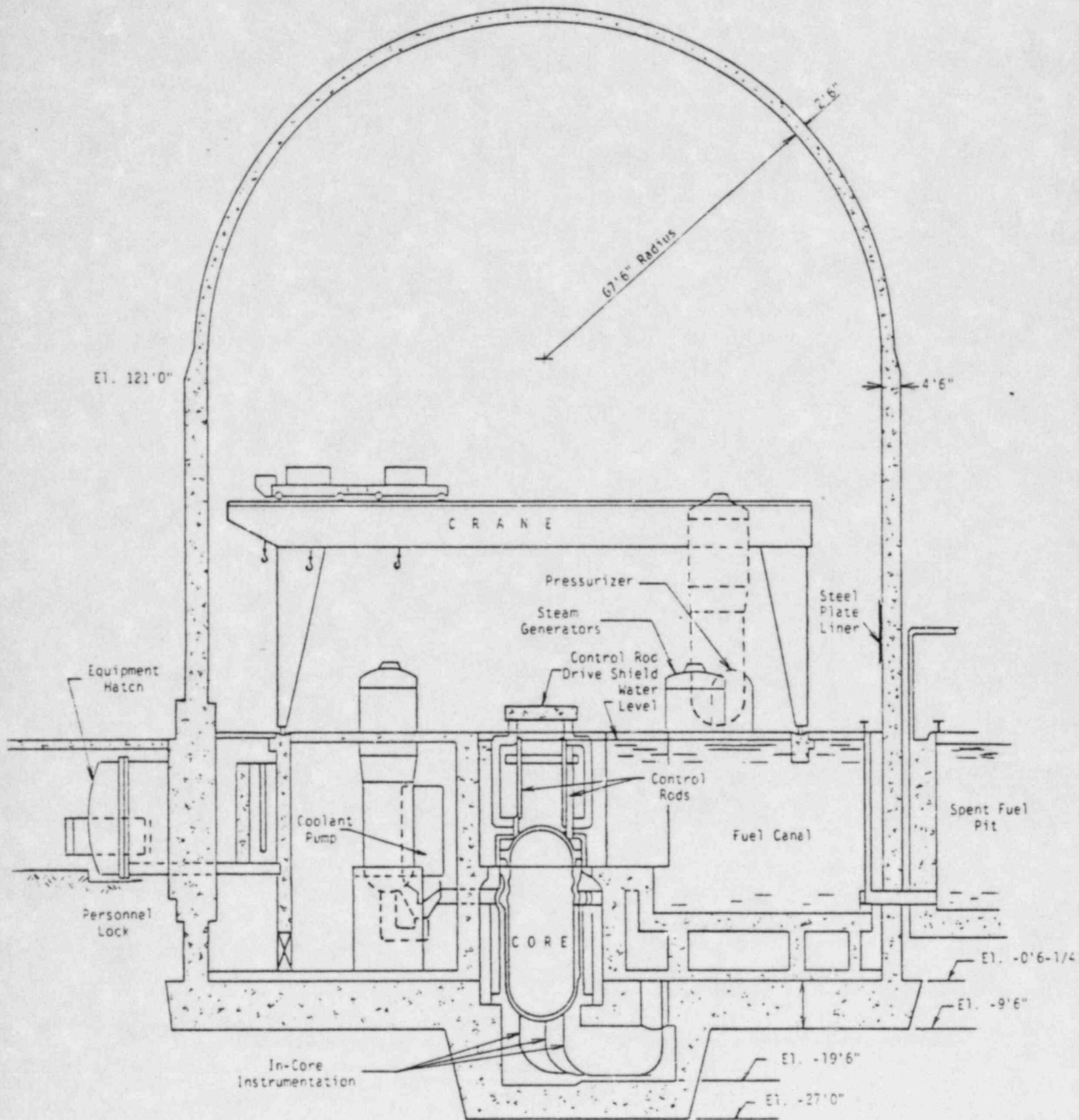


Figure 1. Reactor containment building.

The design strengths of the concrete at 28 days are 3,000 psi for the cylindrical wall and 4,000 psi for the dome. The concrete dome has #18S reinforcing steel bars on both outside and inside surfaces. The concrete cylindrical wall is also reinforced with #18S bars on the outside and inside surfaces in both vertical and hoop directions.

The #18S bars in both dome and cylindrical wall have about 12 in. spacing. There is one layer of bars on the inside and outside surfaces of the dome and the cylindrical wall in the meridian direction. In the hoop direction of the cylindrical wall, the basic reinforcing steel includes two layers of #18S bars on both outside and inside surfaces. In addition to the basic reinforcing steel, the wall is further reinforced with one more layer of #18S bars near the bottom 17 ft in the hoop direction on the outside surface and in the meridian direction on the inside surface. Also additional #18S or #14 rebars in the diagonal direction are provided around the openings of the wall. Reinforcing steel used in the containment structure conforms to ASTM A408 with a minimum guaranteed yield strength of 50 ksi.

The pipe gallery which connects the containment building to the primary auxiliary building is a 46-ft wide and 10-ft 6-in. high box-type structure. The reactor building also has a 23-ft 2-1/2-in. diameter equipment hatch.

The base slab of the containment structure is founded on granitic gneiss bedrock with the slab bottom embedded 30 ft 6 in. below grade.

The interior surface of the concrete shell is lined with 3/8-in. liner plate in the cylindrical portion and 1/2-in. plate in the dome. The carbon steel liner plate conforms to ASTM A442 with a minimum guaranteed yield strength of 32 ksi. The liner plate functions as a gas barrier to prevent uncontrolled release of fission products from the reactor building during operation and also during a large LOCA. The liner is not relied upon to help the concrete maintain its structural integrity.

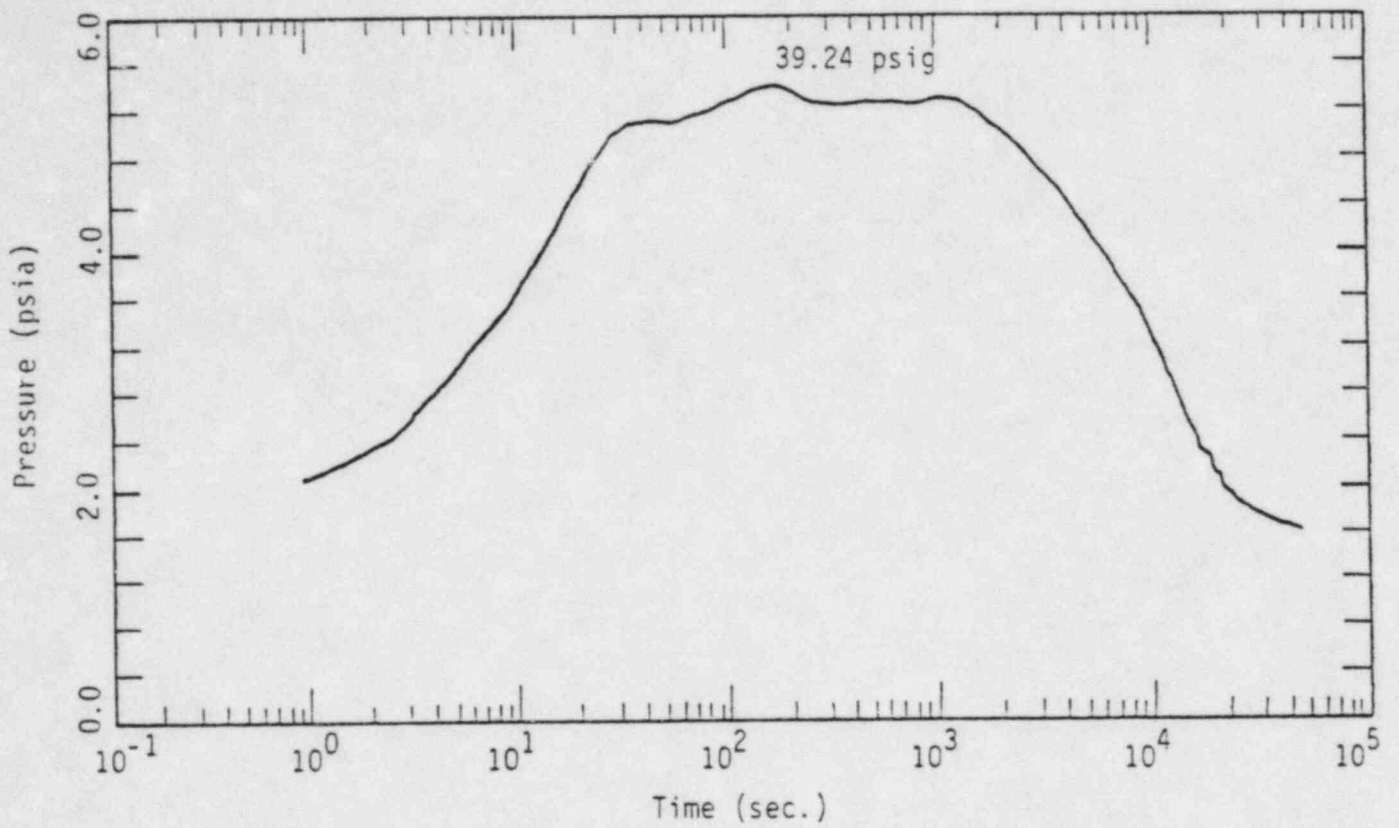
The liner plate is fastened to the concrete wall and dome by Nelson 1/2-in. x 5-3/16-in. H4 concrete anchor studs. On the concrete cylinder, 12,932 studs are arranged in a square diamond pattern, with the rows (or columns) of studs spaced 12 in. apart and staggered; i.e., the studs are in a square pattern in the 45° direction with a stud spacing of about 17 in. For the dome portion of the liner, there are 3,610 studs distributed in 53 rows that are equally spaced 24 in. apart in the meridian direction. There are 11 additional rows of studs (a total of 12,536 studs) in the lower 45° of the dome. Each of these 11 rows contain studs that are spaced approximately 4 in. apart in the circumferential direction.

On the base slab, a 12-1/4-in. thick concrete slab is placed over the liner. The liner is insulated with 2-in. thick polyurethane from base slab to elevation 9 ft 8 in. and 1-in. thick polyurethane between elevation 9 ft 8 in. and 17 ft 8-1/2 in.

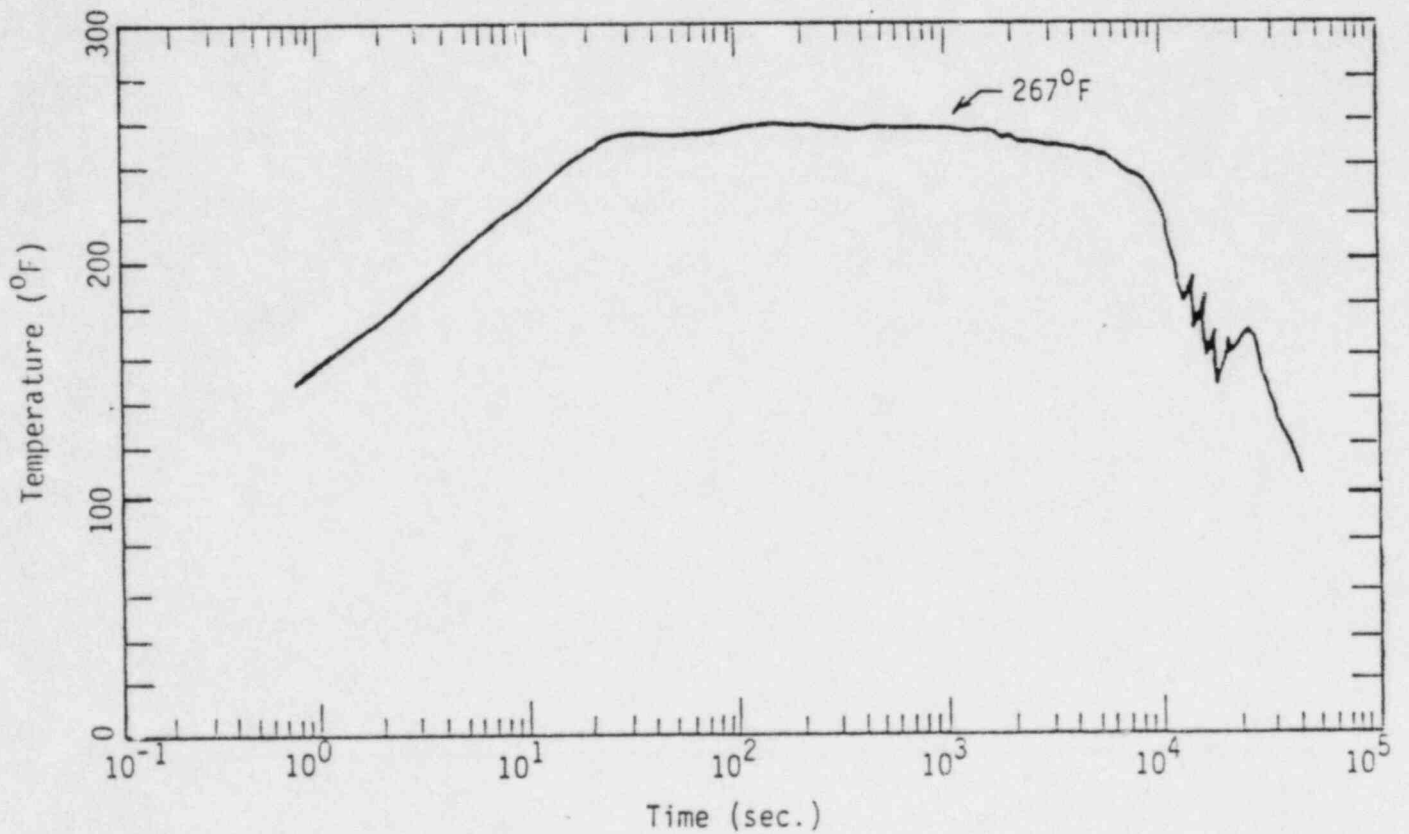
1.3 LOADS AND LOAD COMBINATIONS

The LOCA condition considered in this analysis was based on the information provided in Reference 1. The containment atmosphere pressure and temperature responses of the LOCA are given in Figure 2. The peak atmosphere pressure of 54 psia (or 39.3 psig) occurs at about 100 seconds after the accident, but between 20 seconds and 1,000 seconds the pressure remains almost at constant at about 37 psig. The accident temperature of the containment atmosphere remains around 260°F for a long time (between 20 seconds and 5,000 seconds). The peak temperature is 267°F.

To obtain the temperature gradients through the concrete wall and dome, thermal transient analyses using the computer code ANSYS (Reference 2) were performed. The concrete wall and the dome including the liner plate were assumed to be one-dimensional thermal-transient media with an initial steady-state thermal condition of 120°F on the inside surface of the liner and 3°F on the outside surface of the concrete. The initial conditions were based on the winter operating condition of the containment.



(a) Containment pressure response.



(b) Containment temperature Response.

Figure 2. Containment pressure and temperature response for the loss-of-coolant accident (LOCA).

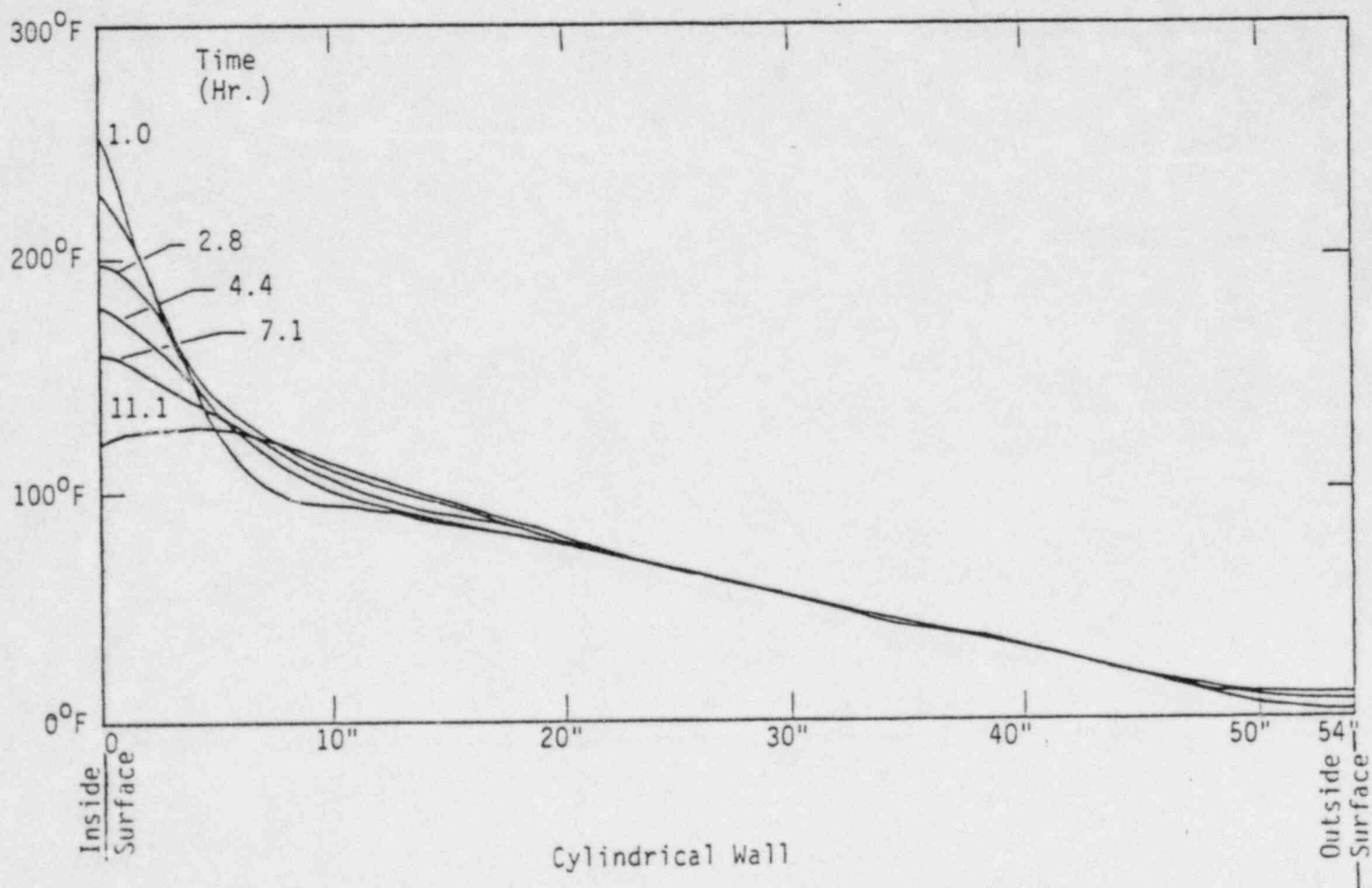
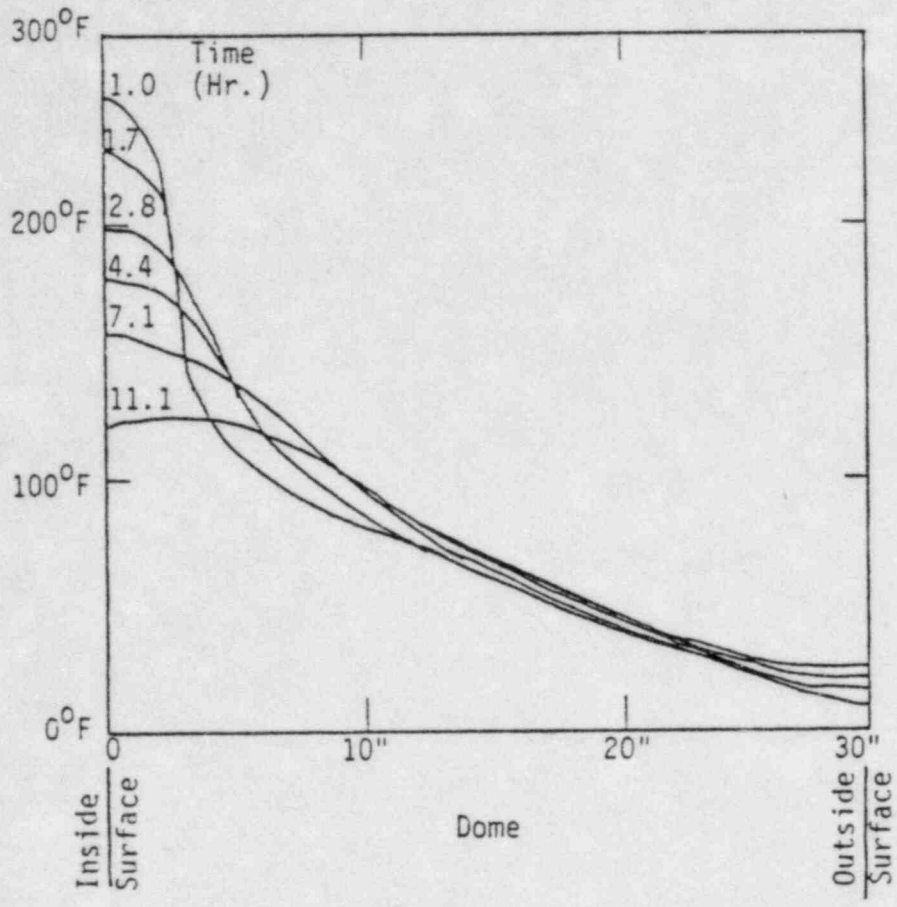


Figure 3. Accident temperature gradients through the uninsulated containment wall and dome.

In the thermal-transient analysis, the liner was assumed to have the same temperature as the containment atmosphere. Three analyses were performed, one for the dome which is 30 in. thick, one for the cylindrical wall which is 54 in. thick, and another for the cylindrical wall with 1-in. insulation. The result of the case of the concrete wall with insulation showed almost no temperature variations in the liner and concrete; they maintained almost the same temperature profile as for the initial condition. The temperature gradients, varying with time, for the two uninsulated cases are shown in Figure 3 which shows the temperature distribution through the thickness of dome and cylindrical wall for different times during the accident.

The seismic condition for the containment structure was based on the site-specific spectra recommended in Reference 3 for the Haddam Neck site with peak ground acceleration of 0.21 g in the horizontal directions and 0.14 g in the vertical direction. The pseudo-acceleration-spectral values for the horizontal and vertical directions of 7% critical damping are listed in Table 1.

Table 1. Site specific spectrum.

<u>Frequency (CPS)</u>	<u>Horizontal Spectrum (in./sec²)</u>	<u>Vertical Spectrum (in./sec²)</u>
1.00	65.92	43.95
2.50	142.41	94.94
3.33	164.09	109.39
5.00	172.99	115.33
10.0	119.33	79.55
12.5	107.03	71.35
20.0	90.13	60.09
25.0	85.0	56.67
33.3	79.72	53.15

Besides the aforementioned LOCA pressure and thermal loads and the SSE load, the only other load considered in the containment-structure analysis was the dead weight of the structure. To combine the different

load cases, a conservative assumption was made; i.e., that the peak responses of the LOCA occur simultaneously with the peak responses of the SSE and that they are combined in the worst fashion.

1.4 MATERIAL PROPERTIES

The material property values used in the analysis are listed in Table 2.

Table 2. Material properties.

	Concrete	Steel Liner (ASTM A-442)	Insulation	Reinforcement Steel (ASTM A-408)
Young's modulus (psi)	3×10^6	30×10^6	---	29×10^6
Poisson's ratio	0.17	0.3	---	---
Weight density (168/ft ³)	150	490	4	---
Coefficient of thermal expansion (in./in./°F)	5×10^{-6}	6.5×10^{-6}	---	---
Thermal conductivity (BTU/hr/in./°F)	0.045	2.17	0.022	---
Specific heat (BTU/lb°F)	0.20	0.11	0.30	---
f'c (concrete compressive strength) (psi)	3,000 (cylinder) 4,000 (dome)	---	---	---
y (Minimum steel yielding stress) (psi)	---	32,000	---	50,000

2. ANALYSIS OF CONTAINMENT SHELL STRUCTURE

2.1 ANALYTICAL MODEL

The containment shell, which is detached from the containment interior structures, is essentially an axisymmetric structure with the exception of the penetrations and the area connected to the pipe gallery. The pipe gallery which connects the containment building to the primary auxiliary building is a 46-ft wide and 10-ft 6-in. high box-type structure. Since the pipe gallery joins the containment shell near its base, the asymmetric effects of the pipe gallery to the containment shell were believed to be minimal in the seismic analysis. Also, the equipment hatch opening as well as other openings on the shell wall were reinforced with either a thickened concrete section or additional diagonal rebars. The asymmetry of the shell due to the pipe gallery connections and openings was assumed to be negligible, and the shell structure was modeled as an axisymmetric structure with uniform properties in the circumference direction.

The containment structure was founded directly on the granitic gneiss bedrock. The effects of soil-structure interaction were considered to be small and were neglected in the analysis. The base of the shell was assumed to be fixed.

In the structural analysis of the containment shell, the concrete section was assumed to remain elastic (no cracking of the concrete). After the force and moment of the section were obtained from the elastic structural analysis, a separate cracked-section analysis was performed. The cracked-section analysis took into account the self-limiting nature of the thermal load.

The liner plates on the inside surface of the containment shell were assumed as not contributing to the overall stiffness of the structure and were not included in the structural analysis mode. However, the additional pressure between the concrete wall surface and the liner plate due to the different thermal expansion in the liner and concrete was included by applying an additional equivalent pressure on the concrete wall.

Based on the above considerations, the selected model for the containment shell included forty axisymmetric shell elements representing the concrete cylindrical wall and the dome. The computer code used for the analysis was ANSYS.² For all load cases, except horizontal seismic loads, the shell elements were those designated for axisymmetric loading. When the excitations were horizontal seismic loads, the elements were changed to those for antisymmetric loading of the first harmonic component.

The structural-damping ratio was assumed to be 7% which was suggested by Newmark and Hall⁴ for reinforced concrete structures subjected to stresses below one-half the yield point.

2.2 METHOD OF ANALYSIS

For the dead-load analysis, the standard static finite-element method was applied.

The seismic responses were computed by the response-spectrum method. The site-specific spectra (Table 1) were input in the horizontal and vertical directions. Since the structure was assumed to be axisymmetric, only the responses of one of the two horizontal seismic input needed to be computed.

The modal responses for each direction were combined by the square-root-sum-of-squares (SRSS) method. The responses for horizontal and vertical seismic excitation were also combined by the SRSS method.

During the LOCA, the temperature of the liner plate was assumed to be the same as the containment atmosphere temperature. The time-varying temperature distributions through the thickness of the dome and the cylinder are those given in Figure 3.

To simplify the analysis procedure for the LOCA, the following three representative cases were selected for analysis, based on the data given in Figure 3. Each case represents a different time of the LOCA, a conservative estimation of the liner temperature, and the assumed linear temperature gradient in the concrete wall for the uninsulated part of the structures and the corresponding pressure on the concrete wall.

Table 3. Selected cases for LOCA.

Case	Time Duration (HR)	Liner Temperature (°F)	Concrete Temperature (°F)				Pressure (psig)
			Cylinder		Dome		
			Inside	Outside	Inside	Outside	
1	0<t<1	267	120	3	120	3	39.3
2	1.0<t<2.8	250	130	8	130	8	26.0
3	2.8<t	200	150	10	160	10	15.0

For the insulated part of the structure, the assumption was that the liner temperature remains about 82°F and the concrete wall had an 80°F-inside and 3°F-outside temperature gradient for all three cases. The stress-free temperature of the concrete was assumed to be 70°F.

The additional pressure on the concrete wall due to differential thermal expansion in the liner and concrete was calculated to be 3 psi for the insulated part. For the uninsulated part of the structure, the estimated additional pressures on the dome and the cylinder were, respectively, 36.2 psi and 14.7 psi for the first case, 33.4 psi and 13.7 psi for the second case, and 22.0 psi and 9.4 psi for the third case.

Each load case for the dead, seismic, pressure, and thermal loads was analyzed individually. The responses, in terms of section forces and moments, were then combined in a fashion which gave the worst condition at the section. At several selected sections along the height of the structure, the stresses in rebars and concrete were calculated using a cracked-section analysis approach which took into account the self-limiting nature of the thermal loads. The details of the cracked-section analysis were given in an earlier SEP report.⁵

2.3 RESULTS OF ANALYSIS

The structural responses, given as the section forces and moments along the height in both meridian and hoop directions, are shown in Figure 4 for the dead-load case.

The first ten anti-symmetric modes (for horizontal excitations) have frequencies ranging from 5.35 Hz to 33.2 Hz. The first three horizontal mode shapes are shown in Figure 5. The first ten symmetric modes (for vertical excitations) have frequencies ranging from 13.6 Hz to 35.3 Hz. Shown in Figure 6 are the mode shapes for the first three vertical modes. Figures 7 through 9 give the seismic responses to SSE.

The structural responses to peak pressure load (39.3 psig) are given in Figure 10. These responses were used for the load combination of Case 1. The responses to pressure loads of Case 2 and Case 3 were obtained by multiplying the responses given in Figure 10 by the factors 26/39.3 and 15/39.3, respectively. The responses due to the thermal loads of Cases 1, 2, and 3, including the effects of the additional pressure due to differential expansion of liner and concrete, are shown in Figures 11 through 13.

The results show that the dominant responses are the thermal and pressure responses during LOCA; the seismic and dead loads have only minor effects.

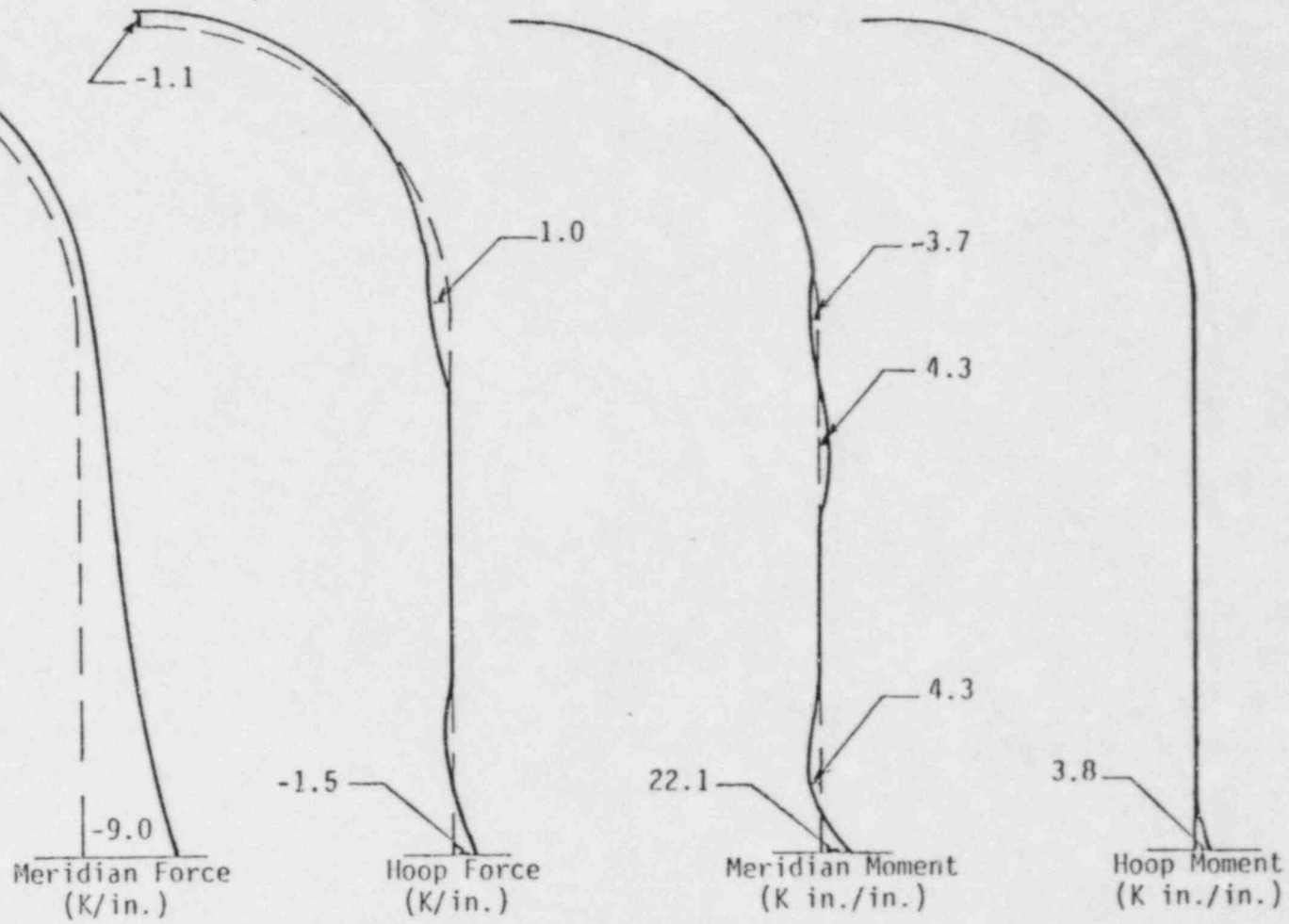


Figure 4. Calculated responses due to dead load.

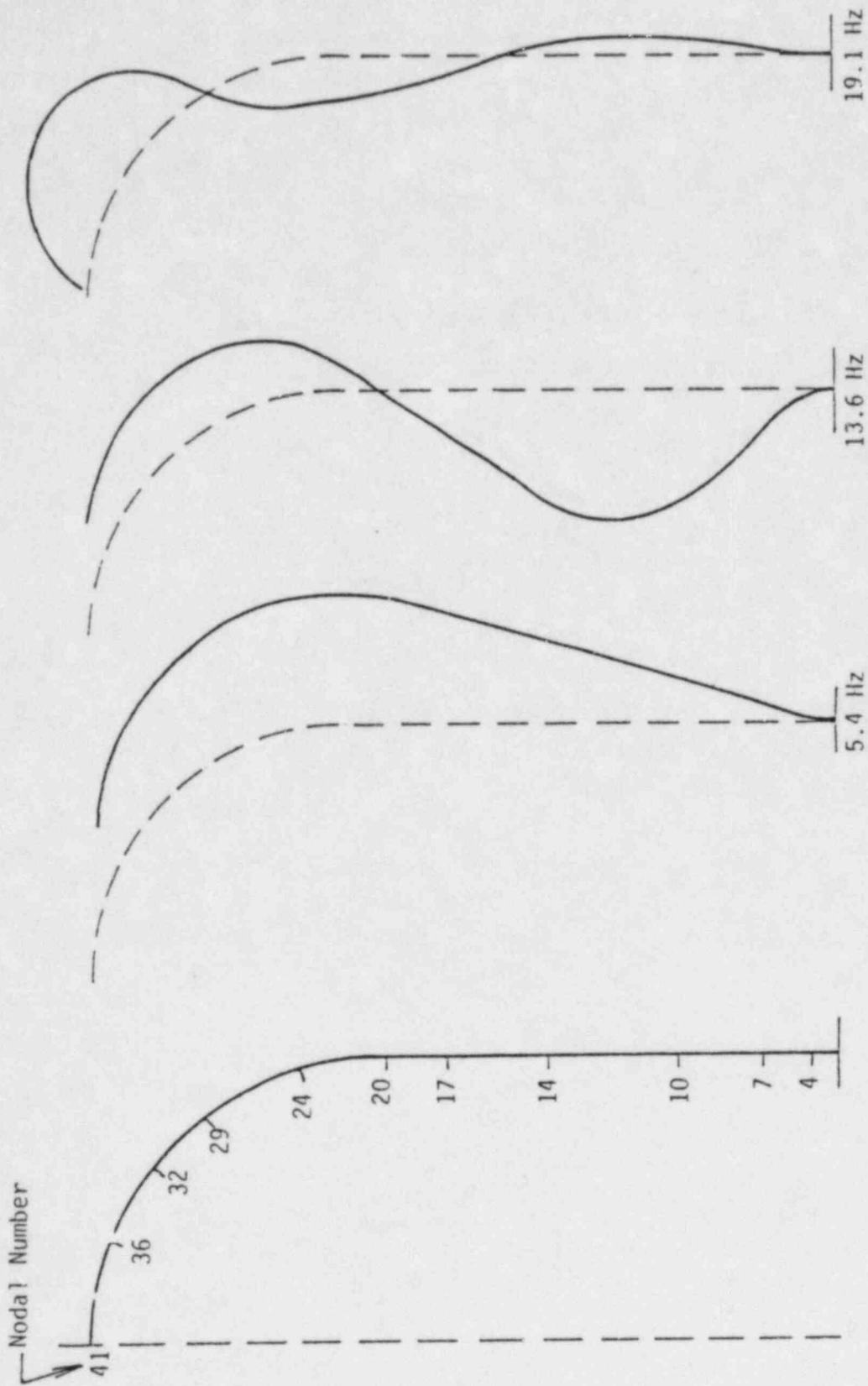


Figure 5. Antisymmetrical mode shapes.

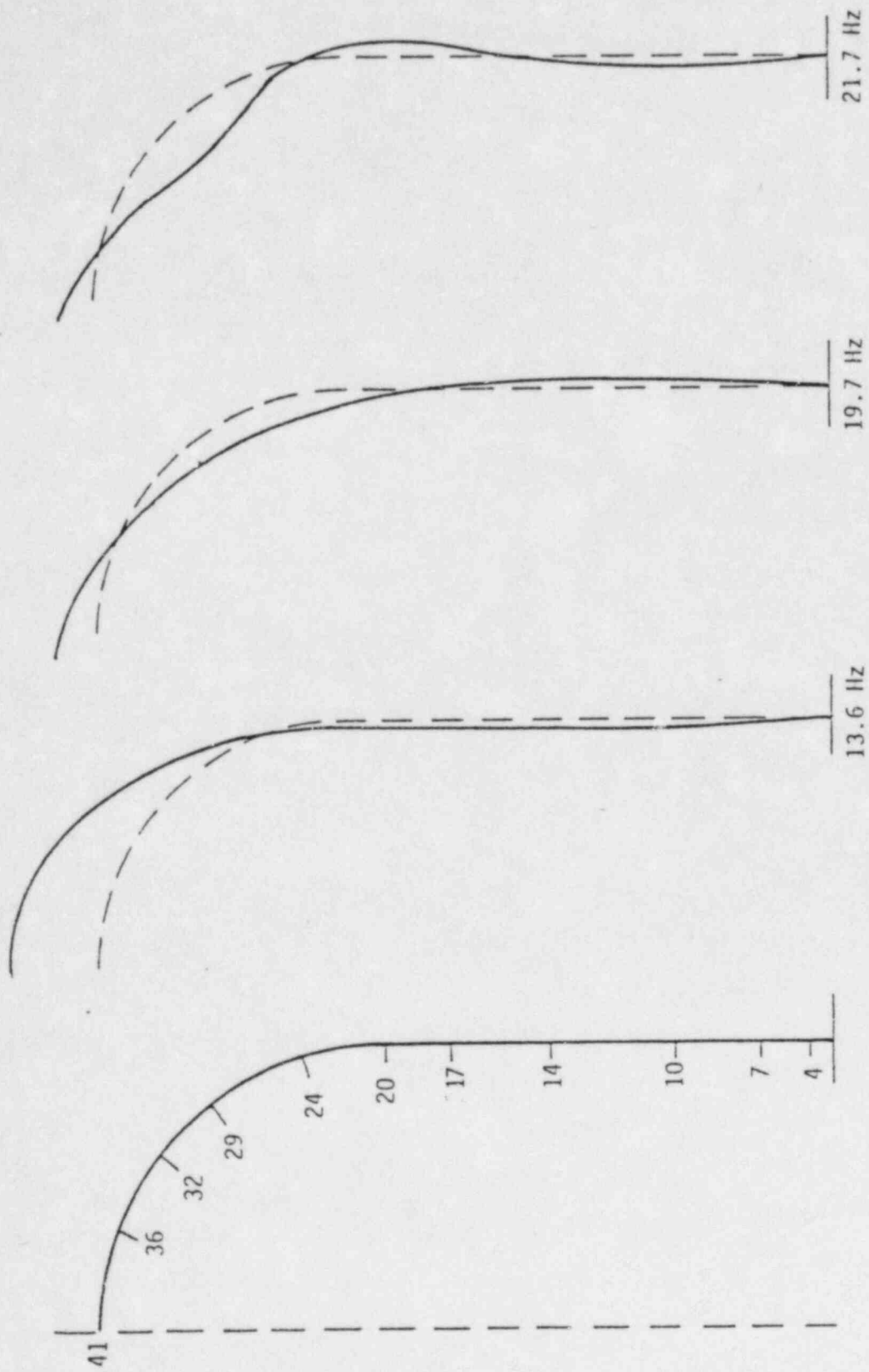


Figure 6. Symmetrical mode shapes.

2-8

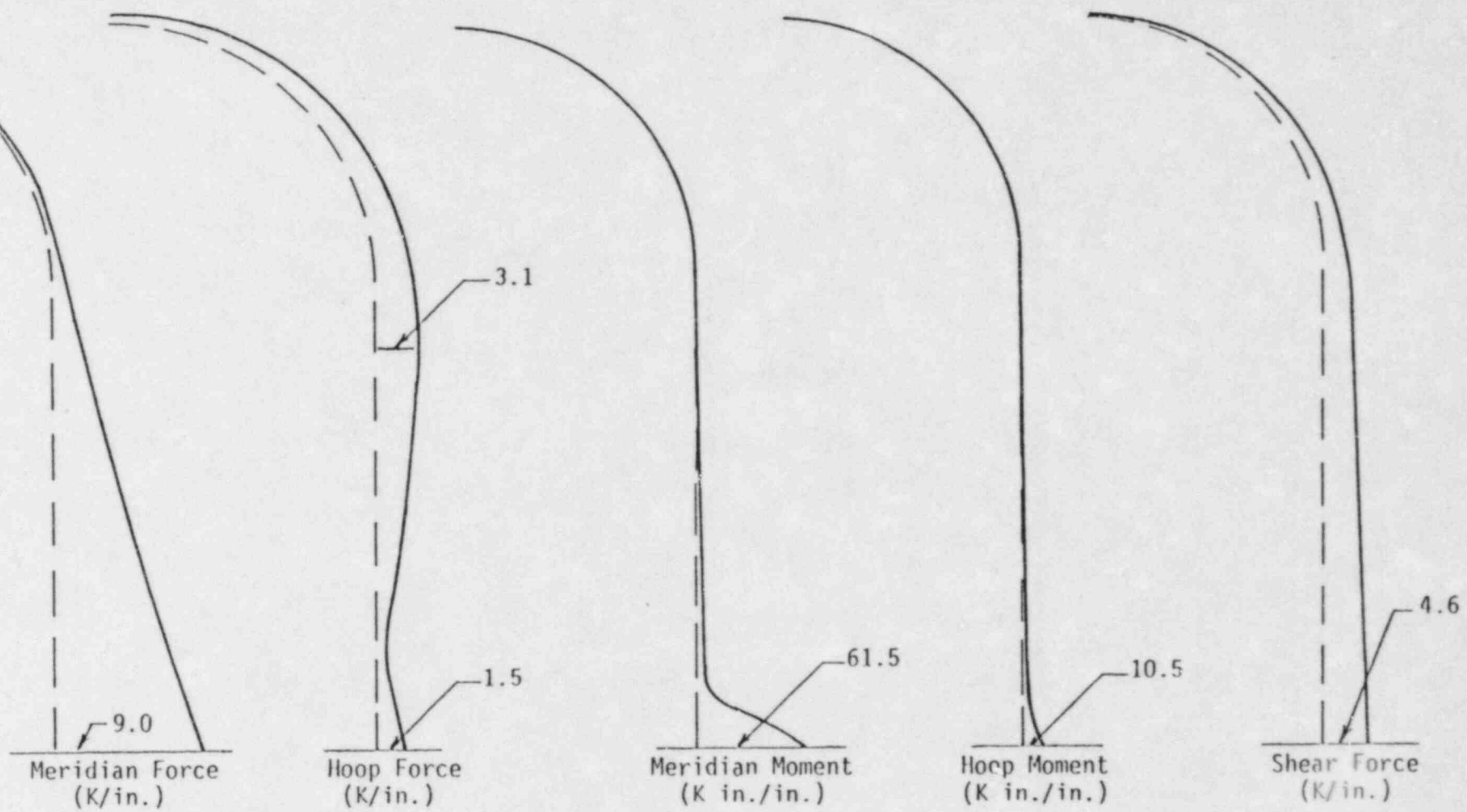
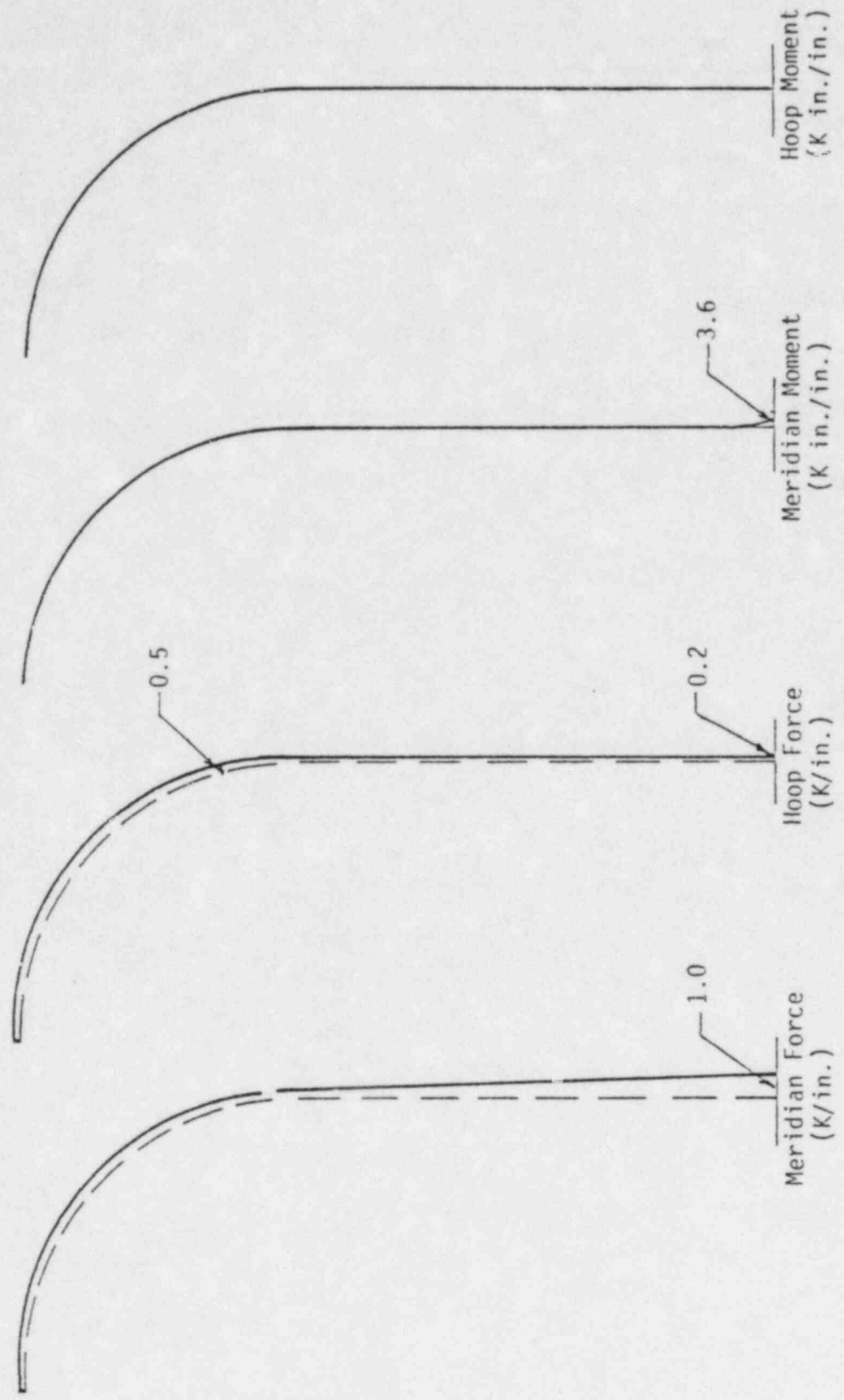


Figure 7. Calculated responses due to horizontal component of SSE.



7
Figure 8. Calculated responses due to vertical component of SSE.

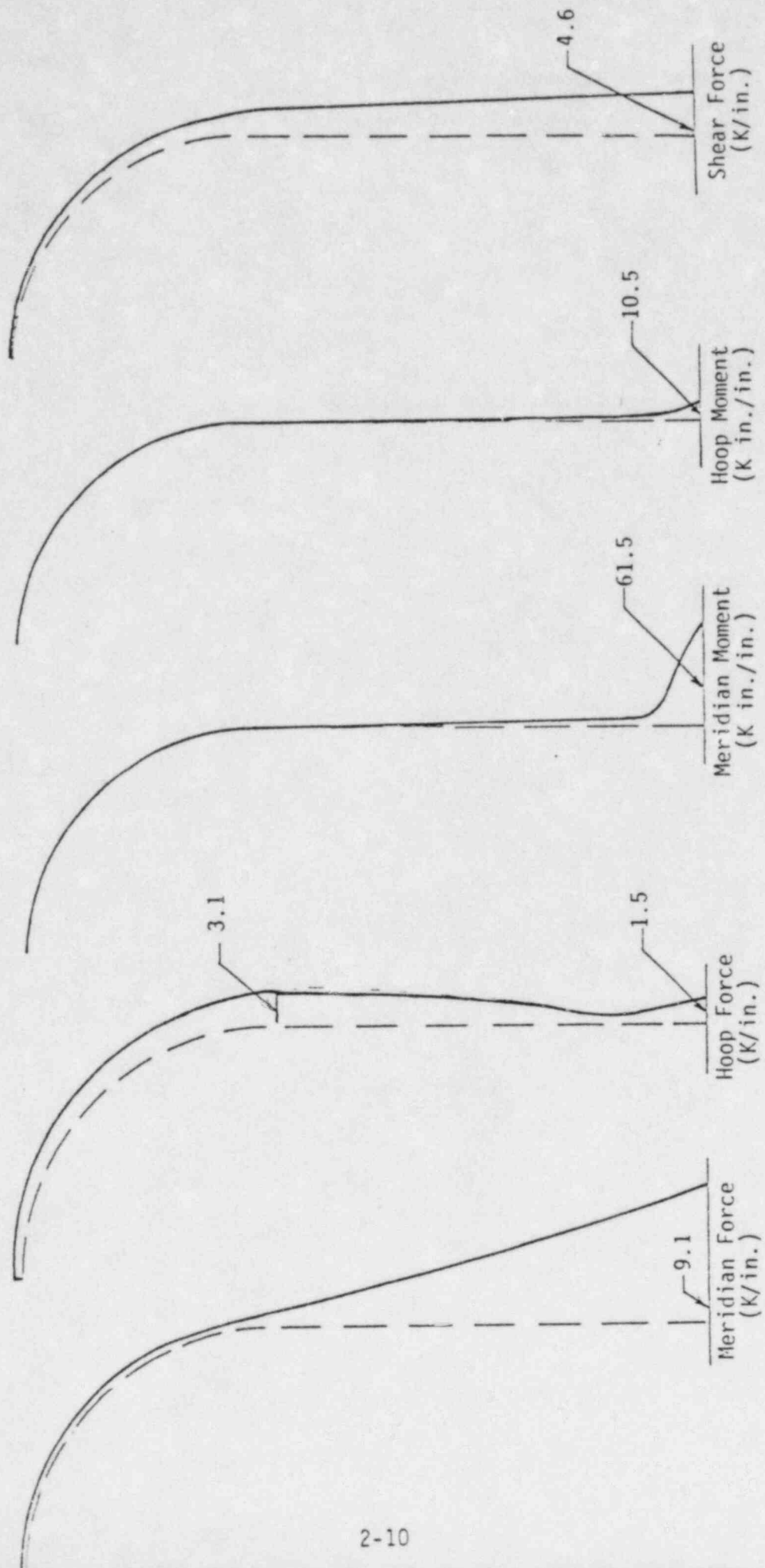


Figure 9. Calculated responses due to SSE.

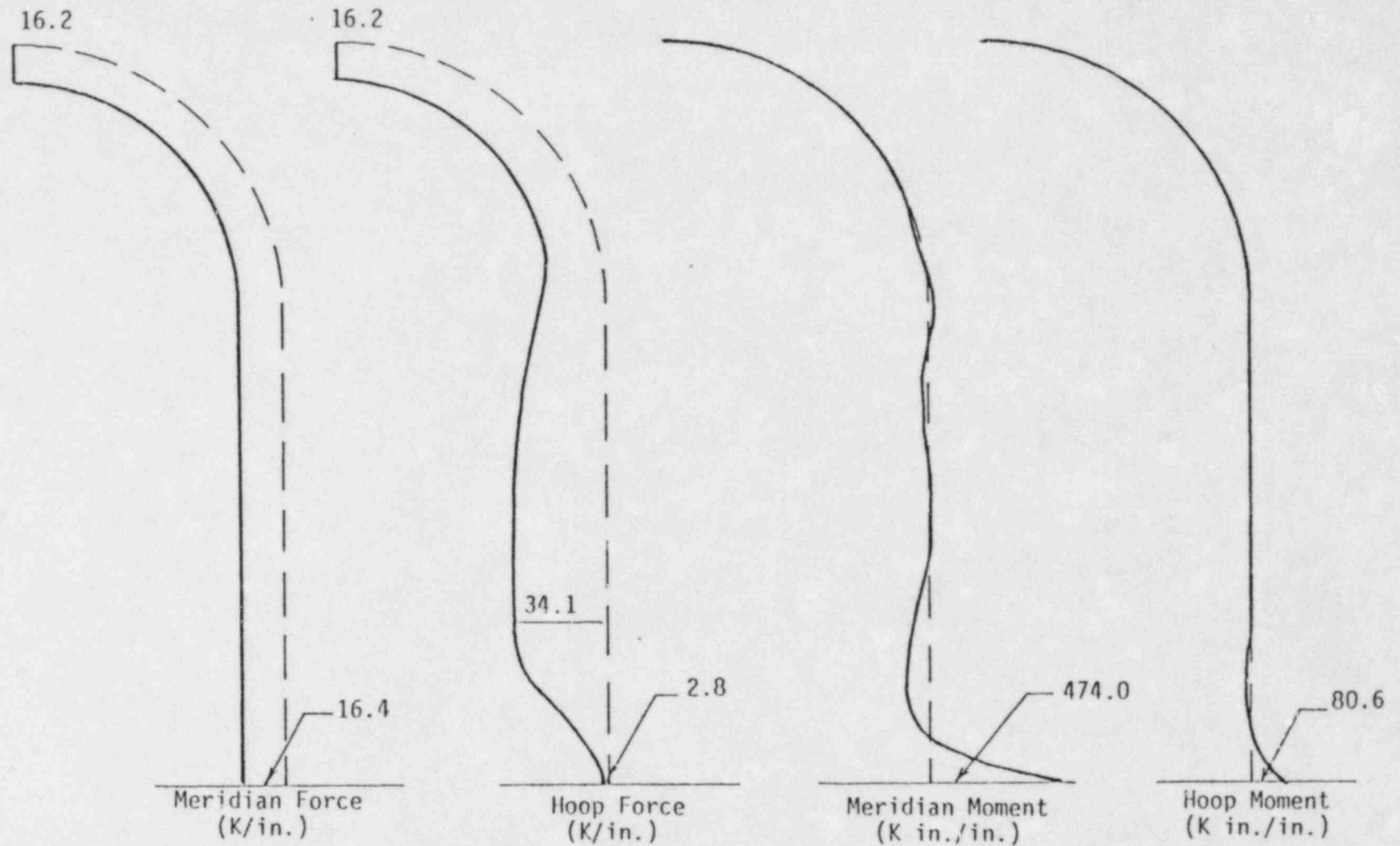


Figure 10. Calculated responses due to pressure load (39.3 psig).

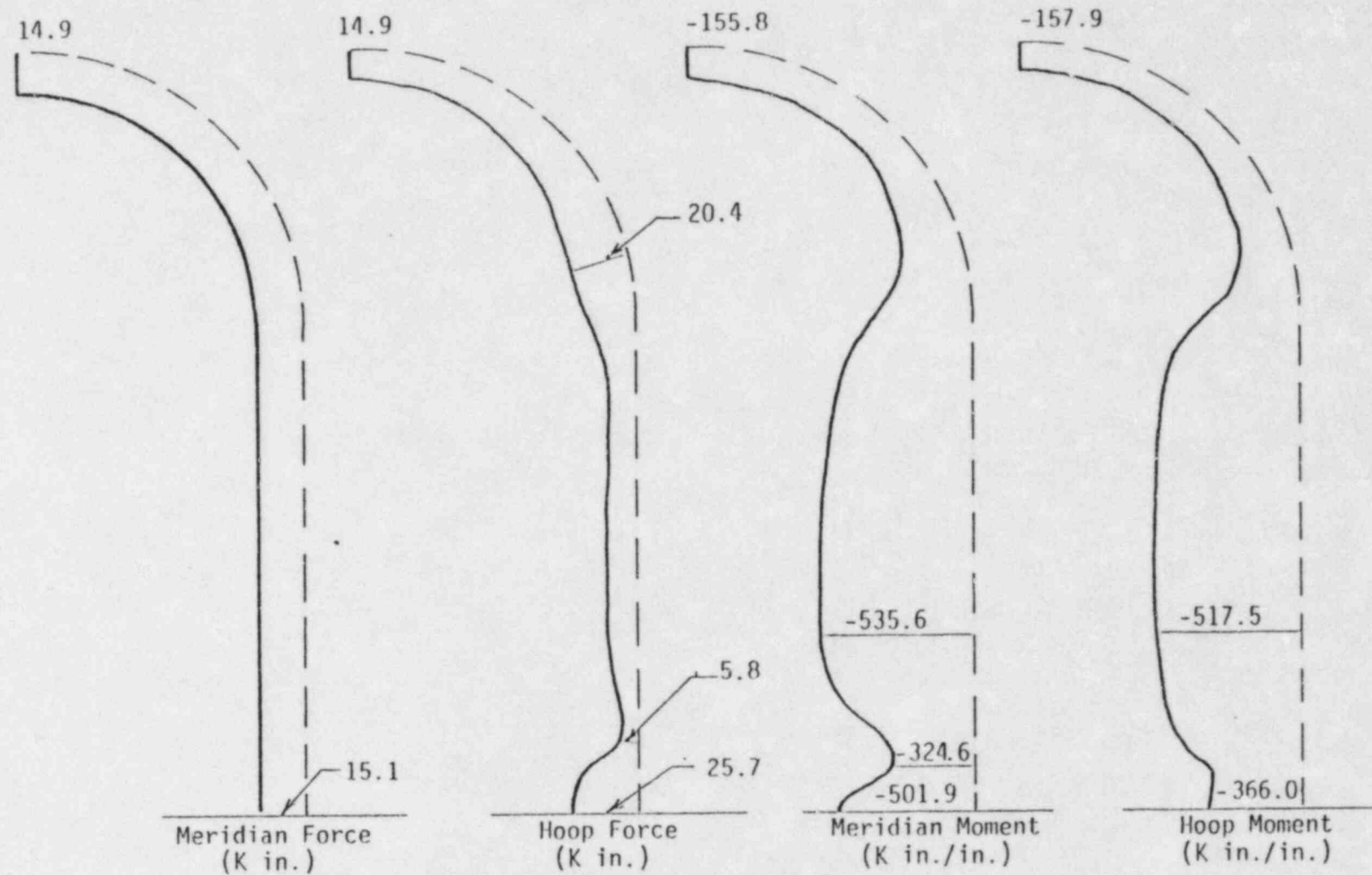


Figure 11. Calculated response due to thermal load of Case 1.

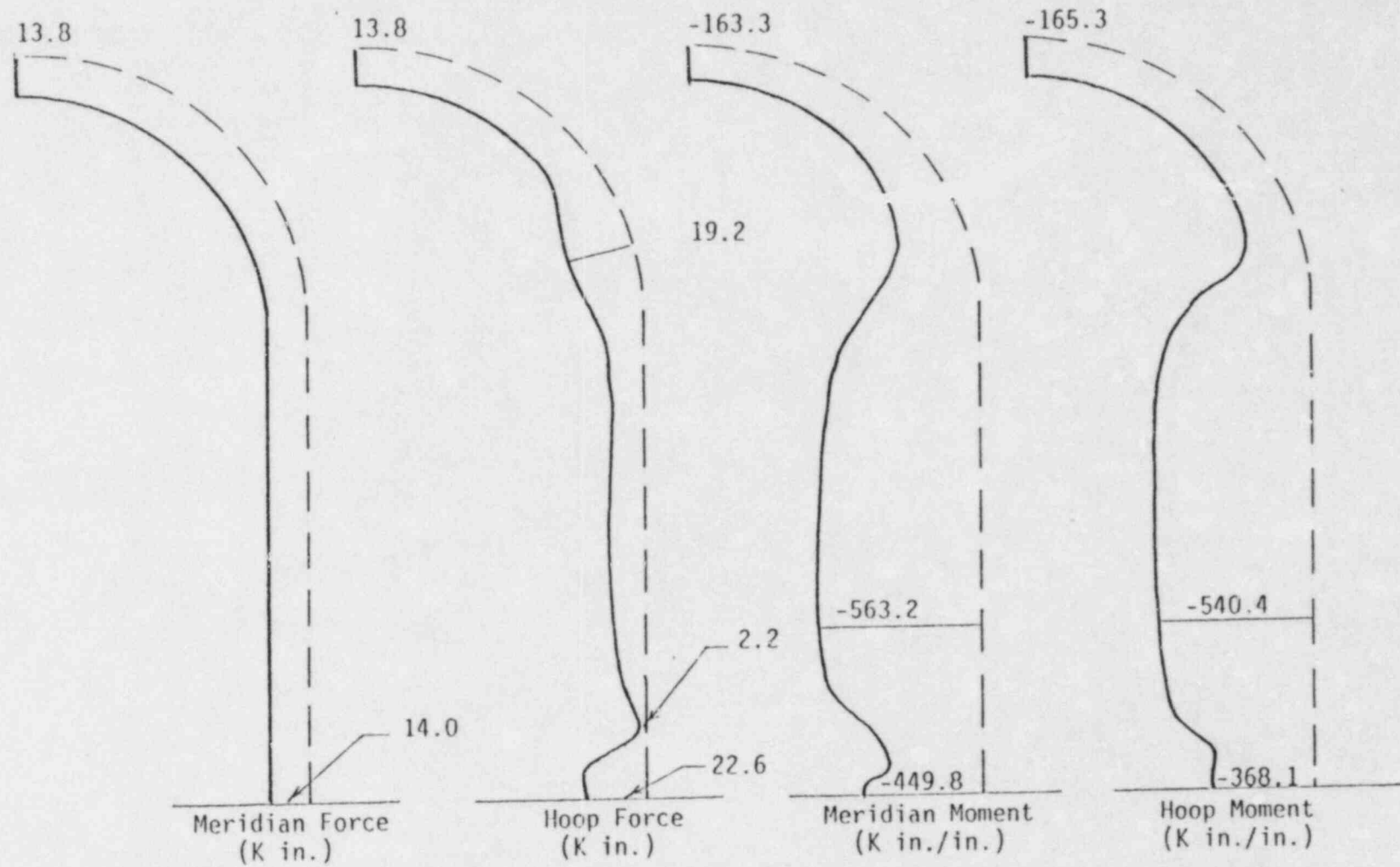


Figure 12. Calculated response due to thermal load of Case 2.

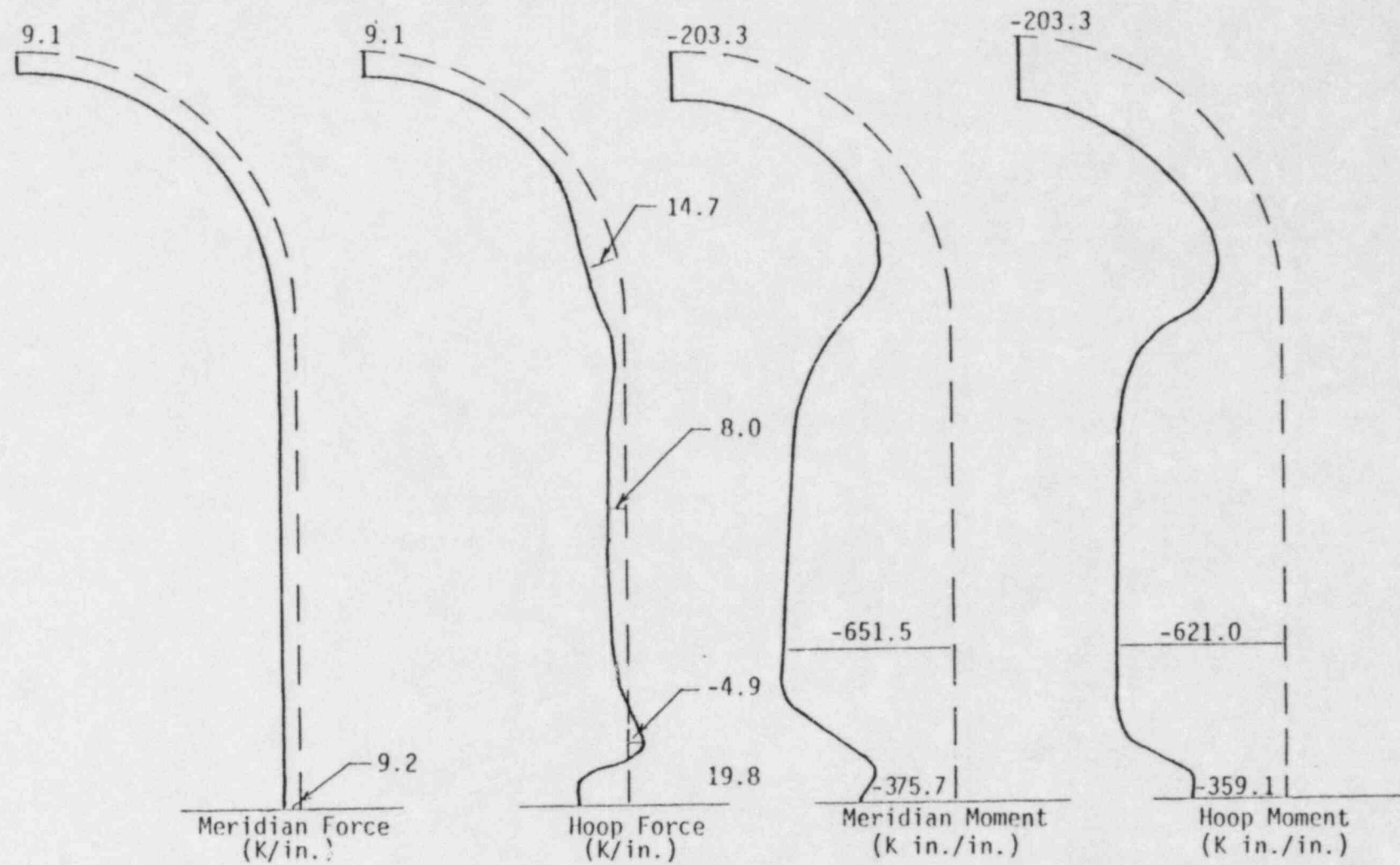


Figure 13. Calculated responses due to thermal load of Case 3.

Cracked-section analyses were carried out at different sections along the height of the structure for each of the three Cases combined with the dead and seismic loads. The results show that in Case 1 (the first hour of the accident), cracks develop through the thickness of the concrete over almost the whole structure. In such case, no significant thermal loads remain in the section, rebars take almost all the loads applied on the section. The highest stress for rebars in the meridian direction was estimated to be 45 ksi. In the hoop direction, the highest rebar stress was 41 ksi. Between hours 1 and 2.8 of the accident (Case 2), cracks still remain through the thickness but the highest meridian rebar stress is 32 ksi and the highest hoop rebar stress is 28 ksi. After 2.8 hours, the highest rebar stresses are 26 ksi and 22 ksi in the meridian and hoop directions, respectively.

The maximum radial shear stress in the containment shell structure was calculated, using thin-shell theory for fixed-base cylindrical shells, to be about 120 psi. ASME Boiler and Pressure Vessel Code, Section III, Division 2, Article CC-3421.4.1, does not allow concrete shear stress for sections subjected to tension. The radial shear has to be taken by the inclined radial reinforcement, #11 rebars at 12-in. spacing. The estimated stress in rebars in this case is 69 ksi which exceeds the yield stress of 40 ksi (ASTM A-15 and A:305).

The maximum tangential shear stress in concrete obtained from analysis was 85 psi near the base. Standard Review Plan 3.8.1 allows only 40 psi for reinforced concrete containment without inclined reinforcements. ASME Code, Article CC-3421.5.1 allows shear up to 160 psi, if the roughness of the crack surface is sufficient to develop the shear capacity along the crack without excessive slip. However, it is believed that significant cracks will develop after LOCA. Therefore, if the postulated LOCA and SSE occur simultaneously or consecutively, the containment structure has to rely on the liner to take the extra shear force. The estimated additional liner shear stress is 6.5 ksi, in this case.

3. ANALYSIS OF THE LINER SYSTEM

3.1 ASSUMPTIONS

Most of the loads imposed on the liner plate result from strains in the liner due to deformation of the concrete shell. In the event of an accident temperature, the temperature in the liner plate will be higher than the average temperature in the concrete shell. Restrained by the stud anchors from expanding more than the concrete shell, the liner plate is then subjected to a membrane compression force due to the thermal load. In any case, the anchors will hardly be loaded unless the membrane loads developed in any two adjacent panels of the liner do not balance each other.

The insulation that lines the inner face of the liner plate at the lower portion of the containment will cause a temperature differential in the liner plate at the upper edge of the insulation. This causes an unbalance in the liner membrane forces at this location in the meridian direction, and the studs there will be subjected to a net downward shear load. In addition, any imperfection in fabrication and erection of the liner plate such that one panel is bent with an initial inward curvature will also cause an unbalance in the liner membrane forces. This is due to the in-plane stiffness of a bent plate being less than that of a flat plate, and the anchors will deform laterally toward the bent plate. The anchor at where the unbalanced forces occur will be stressed the most, and the remaining anchors will be subjected to loads that diminish with the distance from the most stressed anchor.

As described in Section 1, the stud anchors are arranged in a square diamond pattern. For the purpose of analysis, the diamond pattern is rotated by 45 degrees so that it becomes a square pattern in the meridian or circumferential direction while the anchor spacing of 17 in. remains unchanged. This simplification does not materially alter the actual capacity of the liner system, but allows a one-dimensional analysis for a

17-in. wide strip of the liner system in the meridian or hoop direction. The one-dimensional analysis is conservative because the benefit of biaxial stiffness of the liner plate is not taken into account.

Two cases were considered. Case 1 considered a strip of the liner in the meridian direction, 17-in. in width and consisting of both the insulated and uninsulated portions of the liner system. All plates in the strip were assumed to be perfectly flat (Figure 14). Case 2 considered a circumferential strip of the uninsulated liner immediately above the insulation, also 17-in. in width. The liner was assumed to be perfectly flat except for one panel which was initially bent, having an inward curvature and an initial deflection at the center of the panel equal to $\Delta_m = 1/4$ in. (Figure 15).

3.2 INITIAL MEMBRANE LOADS IN LINER PLATE

For the effect of creep and shrinkage of the concrete (S) and for the mechanical loads such as dead weight (D), SSE seismic load (E) and accident pressure (P), the resultant strains in the concrete shell inner surface essentially represent the strains that would be induced in the liner because of the restraints from the stud anchors. For the effect of concrete shrinkage, a typical strain of $e_z = e_h = -100 \mu$ in the meridian and hoop directions was assumed. For D, E, and P, the liner strains were computed from the forces and moments in the concrete shell. Section 2 provides the per unit length meridional force (f_z) and moment (M_z), and per unit length hoop force (f_h) and moment (M_h) for the D, E, and P loads.

The forces and moments in the concrete due to D, E, and P were then combined, from which the inside fiber stresses in the concrete shell can be determined:

$$s_z = f_z/t + 6M_z/t^2 \quad (3-1)$$

$$s_h = f_h/t + 6M_h/t^2$$

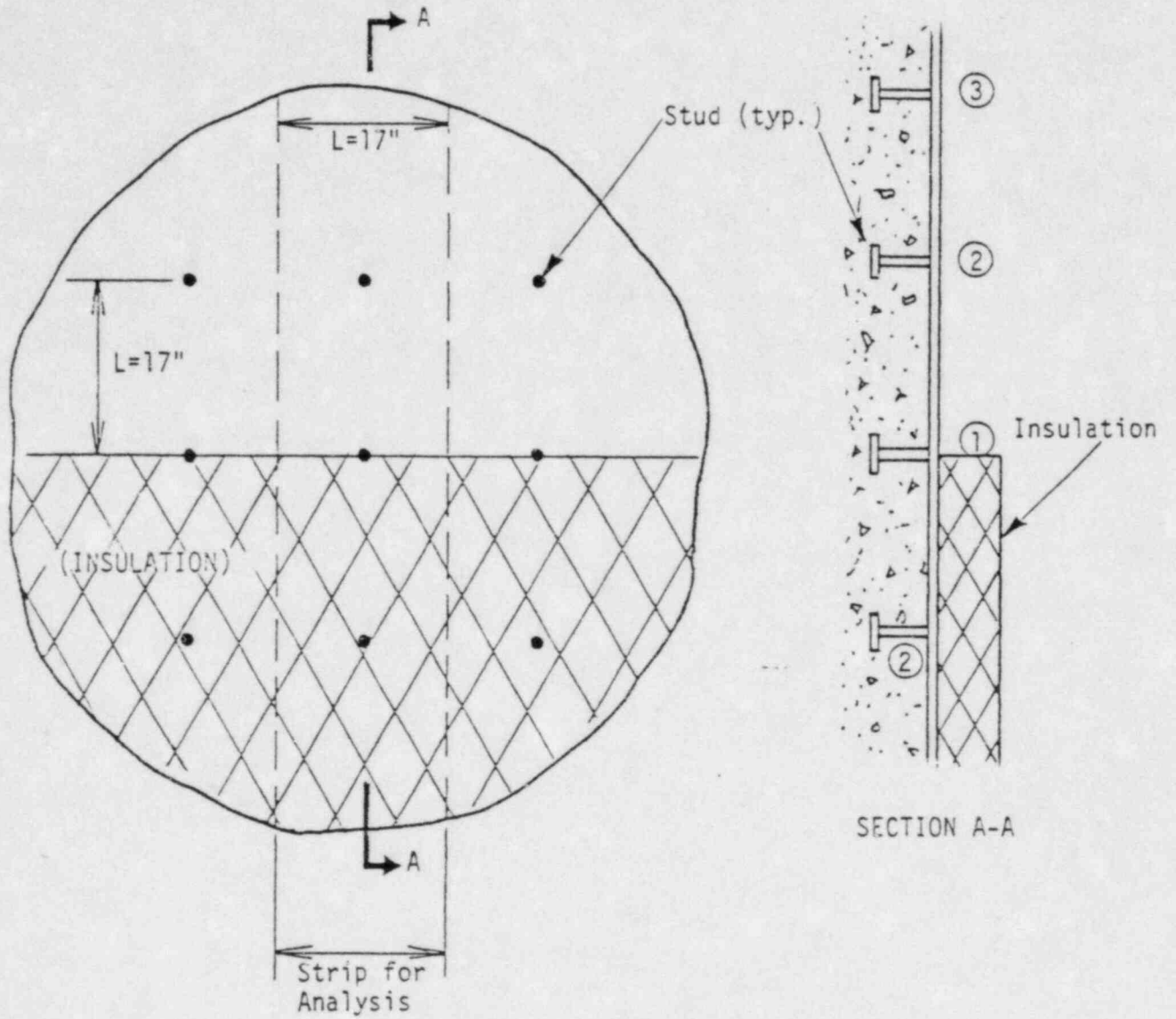


Figure 14. Analysis Case 1 - a meridional strip of flat liner system.

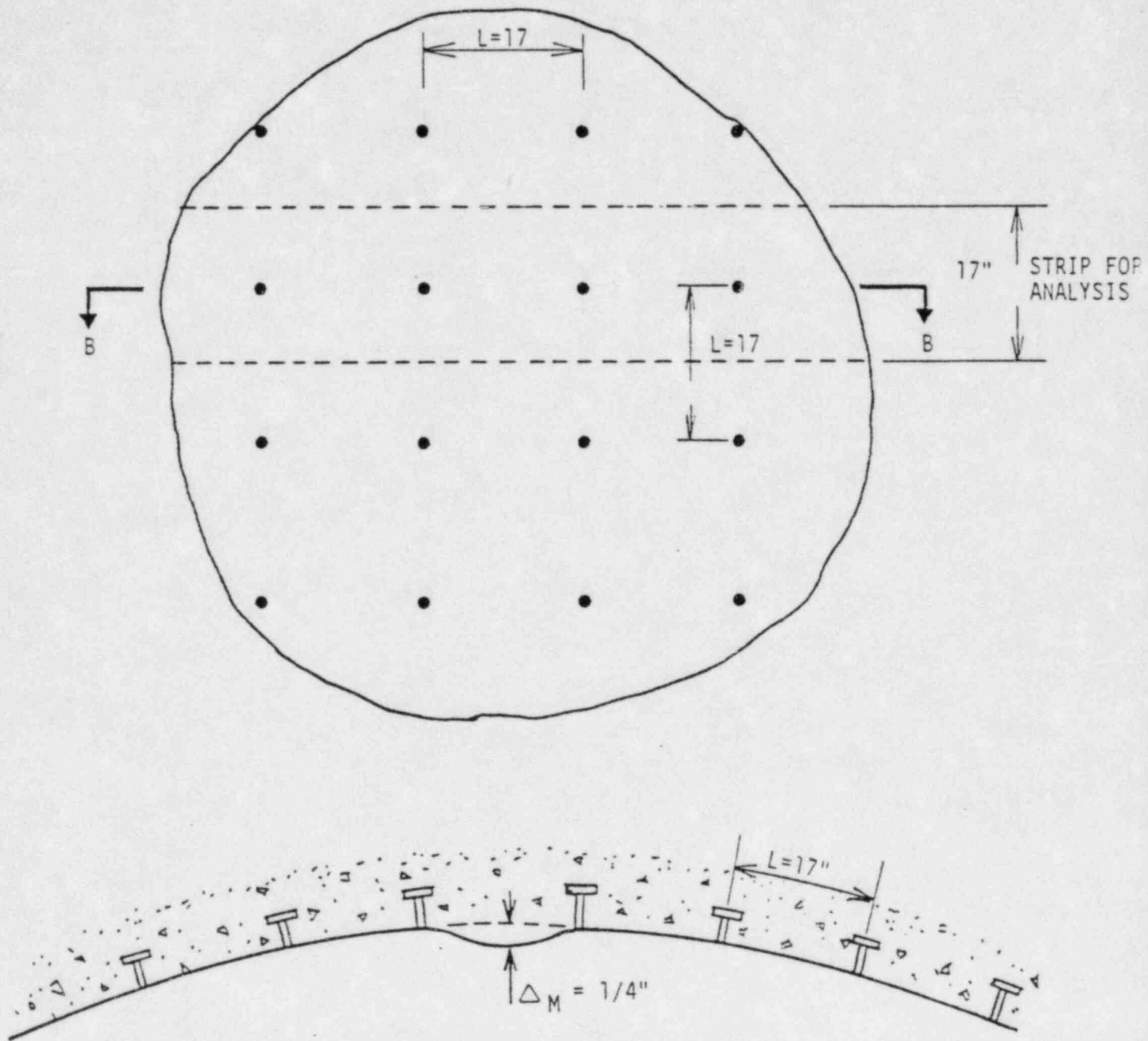


Figure 15. Analysis Case 2 - a circumferential liner strip with a bent plate.

In Eq. (3-1), t is the liner plate thickness (3/8 in.) and a positive M produces a tensile bending stress at the inner fiber of the shell. The concrete inner-fiber strains, and hence the liner strains, were determined by the following expressions:

$$e_z = (s_z - 0.17s_h)/E_c \quad (3-2)$$

$$e_h = (s_h - 0.17s_z)/E_c$$

in which 0.17 and E_c are the Poisson's ratio and Young's modulus of the concrete, respectively.

The membrane forces induced to the liner due to the thermal load can be computed based on some equivalent compressive strains. These equivalent strains are equal to the difference in free thermal expansion between the liner and concrete shell. Thus, for thermal loads:

$$e_z = e_h = -6.5 \times 10^{-6} (T_{\text{liner}} - [(T_{\text{conc}})_i + (T_{\text{conc}})_o]/2) \quad (3-3)$$

in which $(T_{\text{conc}})_i$ and $(T_{\text{conc}})_o$ denote the inner and outer face temperatures, respectively, of the concrete shell.

From the liner strains, the membrane forces in a strip of the flat plate become:

$$N_z = E_s L t (e_z + 0.3e_h)/(1-0.3^2) \quad (3-4)$$

$$N_h = E_s L t (e_h + 0.3e_z)/(1-0.3^2)$$

in which E_s and 0.3 are the Young's modulus and Poisson's ratio, respectively, of the liner, and L is the width of the strip. Note that the calculated membrane force must be replaced by the yield load of the plate if the latter is exceeded by the former. The yield load is equal to $N_y = 32 \text{ ksi} \times 17 \times 3/8 = 204 \text{ kip}$.

For a bent plate within the liner strip, it was conservatively assumed that only the accident pressure load, P, contributes to the initial forces. From Reference 5, the pressure induces a compressive membrane force in the liner strip that can be approximately given by:

$$N'_h \text{ (or } N'_z) = -PL^3/2\pi^2\Delta_m \quad (3-5)$$

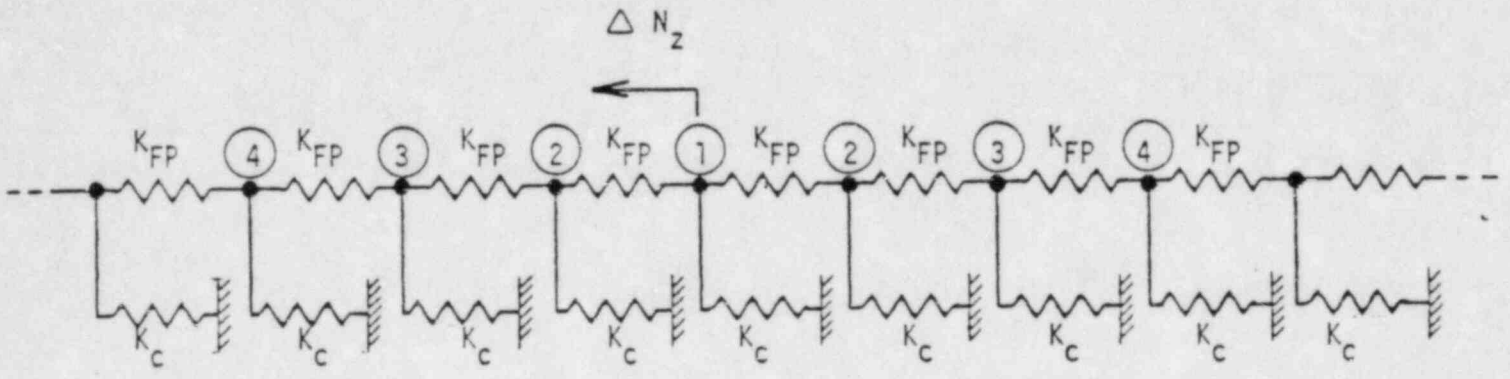
in which Δ_m is the initial inward deflection at the center of the bent plate, and L = 17 in.

3.3 ANALYSIS MODELS AND UNBALANCED FORCES

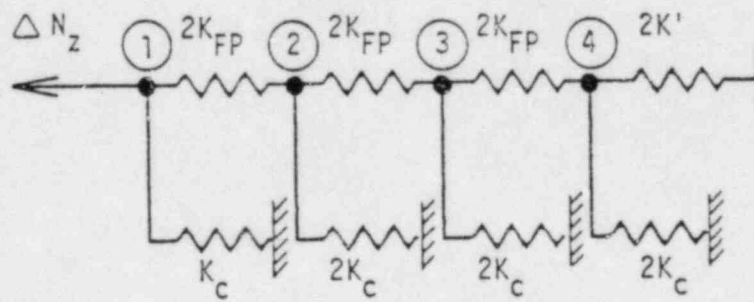
3.3.1 Case 1 - Meridional Strip of Flat Liner Across the Insulation

Figure 16(a) illustrates the analysis model for the meridional strip of liner previously shown in Figure 14. It consists of a series of nonlinear spring elements, K_{FP} and K_C . K_{FP} represents the in-plane stiffness of the flat plate between two studs (Figure 17). It was idealized as an elastic-plastic element. Approximate derivation of the elastic spring stiffness is given in Appendix A. K_C represents the lateral stiffness of the stud anchor as embedded in the concrete. It was adopted from the test data provided by the stud manufacturer⁶. Figure 18 shows the piecewise linearized form of K_C as a function of the lateral deformation, d, of the stud. Note that the ultimate load and displacement of the stud under consideration are $V_U = 14.4$ kips and $d_U = 0.167$ in., respectively.

It was assumed that only three panels of the liner system on each side of the most stressed stud (i.e., stud No. 1) might be stressed into the nonlinear range due to the unbalanced force ΔN_z . The remaining plates and anchors, assumed to remain linear, can be reduced to one equivalent spring, K' (Figure 16(b)). Appendix B presents the derivation for K' and shows that, for $K_{FP} = 6970$ k/in. and $K_C = 400$ k/in., $K' = 1510$ k/in.



(a) Spring Element Model



(b) Equivalent Model.

Figure 16. Analysis model for Case 1.

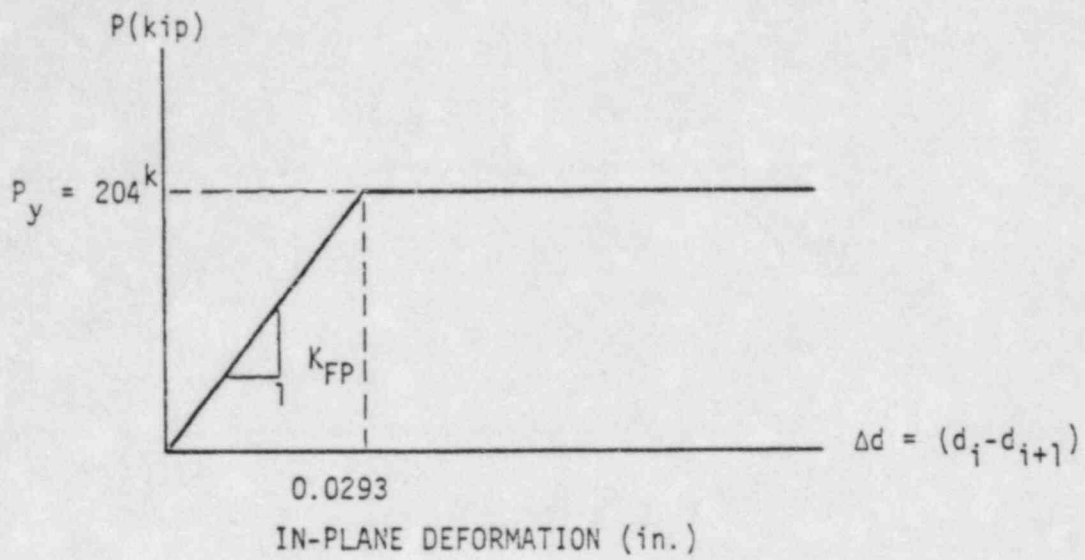


Figure 17. In-plane stiffness for a flat plate.

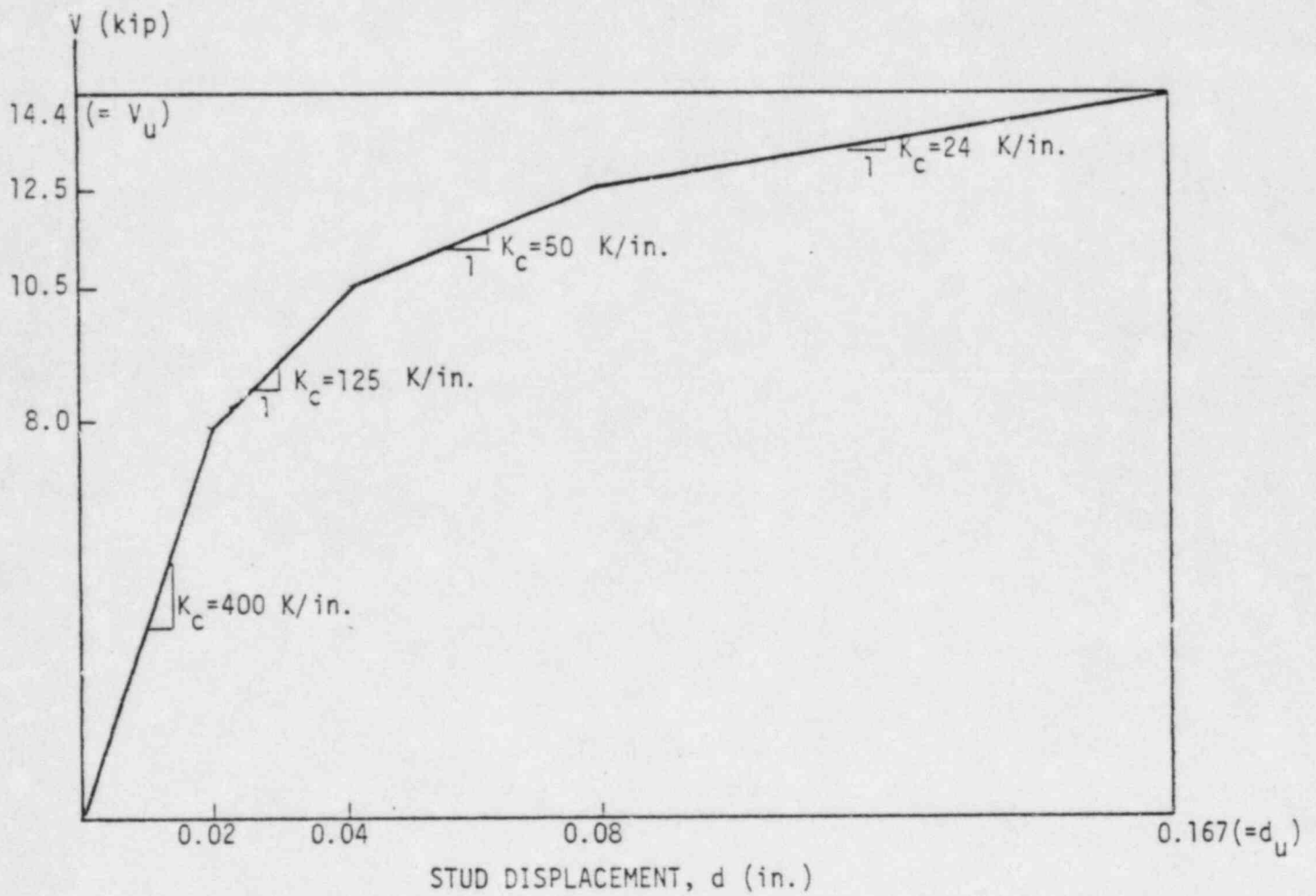


Figure 18. Lateral stiffness K_c for a stud in the concrete.

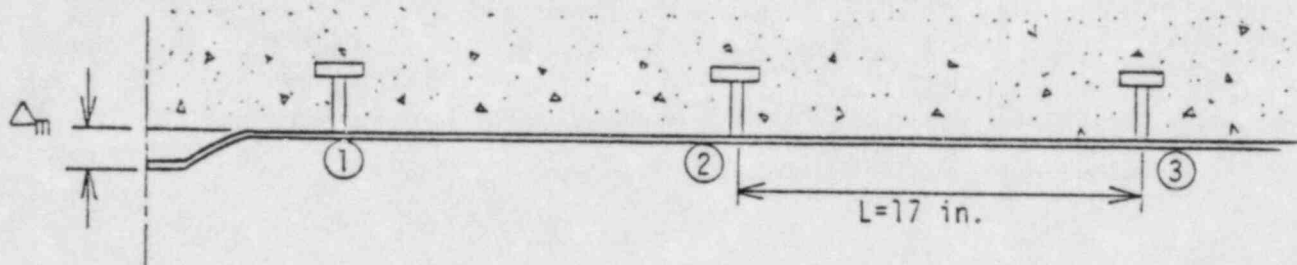
The unbalanced force, ΔN_z , acting downward, represents the difference in the membrane force N_z between the uninsulated and insulated plates. The forces and moments at elements 4 and 6 in the finite element model of the concrete shell (Figures 6, 9, and 10) were used to compute the liner strains in the insulated and uninsulated plates for the combined loads of D, E, and P. Table 4 summarizes the concrete shell forces and moments per unit length for the loads D, E, P, and their combination. The concrete inner face stresses, s_z and s_h , and strains, e_z and e_h , are shown in Table 5. They were computed in accordance with Eqs. (3-1) and (3-2). The liner strains due to the thermal load T were computed from Eq. (3-3), using the following temperature data:

	T_{liner}	$(T_{\text{conc}})_i$	$(T_{\text{conc}})_o$
Insulated Liner	82°F	80°F	3°F
Uninsulated Liner	267°F	120°F	3°F

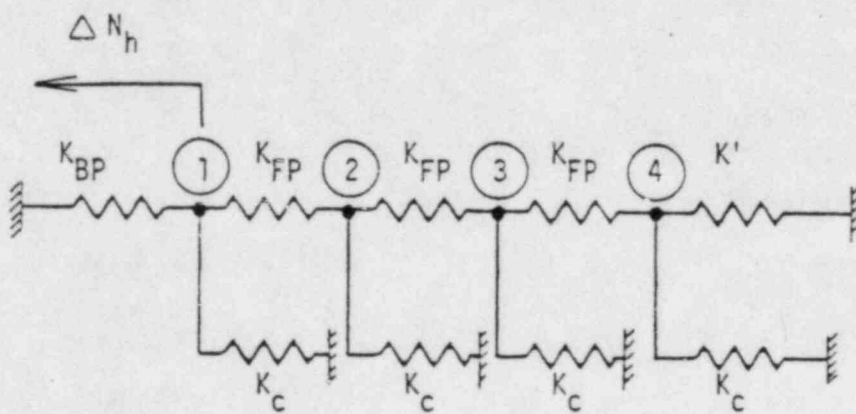
Table 6 shows the membrane force, N_z , as computed from Eq. (3-4). Note that the computed value of 420 kips for the uninsulated plate exceeded the yield force of 204 kips and hence the latter governed for the load combination of D+E+P+S+T. The unbalanced force, ΔN_z , is also shown in Table 6.

3.3.2 Case 2 - Circumferential Liner Strip With One Bent Plate

Because of the symmetry about the center of the bent plate, it sufficed to consider only one half of the liner strip shown in Figure 15 (See Figure 19a). The analysis model can be represented by the spring elements shown in Figure 19(b). It is similar to the analysis model for Case 1, with the exception that a K_{BP} was used to represent the in-plane stiffness of the bent plate. Appendix C shows the derivation for K_{BP} assuming that the plate has yielded flexurally due to membrane loads developed in the plate. Figure 20 shows the stiffness K_{BP} as a function of the in-plane compressional deformation at the edge of the bent plate, d_1 (i.e., the deformation of anchor No. 1).



(a) The Idealized Liner System.



(b) Equivalent Spring Element Model.

Figure 19. Analysis model for Case II.

From the liner strains given in Table 5, the circumferential membrane force in the flat plate can be determined:

$$N_h = -322 \text{ kips}$$

Because the above membrane force exceeded the yield force ($N_y = 204$ kips), the latter governed.

As stated before, it was assumed that only pressure induced an initial membrane force in the bent plate, given by Eq. (3-5):

$$N_h' = 39 \times 17^3 / (2\pi^2 \times 1/4 \times 1000) = -39 \text{ kips}$$

Thus,

$$\Delta N_h = -204 - (-39) = -165 \text{ kips}$$

3.4 ANALYSIS AND RESULTS

Case 1 - Because both K_{FP} and K_C in the analysis model shown in Figure 16(b) might go into the nonlinear range, an iterative procedure was used in the analysis. As a first-trial solution, all K_{FP} and K_C were assumed to be linear. When any one of the K_{FP} and K_C went beyond the linear limit, the solution was iterated until equilibrium was reached. Table 7 lists the final solution for the maximum deformation and anchor load at anchor No. 1, d_{max} and V_{max} respectively, and the maximum liner strain.

Case 2 - The analysis procedure is similar to that employed in Case 1. The bent-plate membrane force was iteratively selected from Figure 20, based on the iterated solution for d_1 . The results of the analysis for the load combination D+E+P+S+T are listed in Table 7.

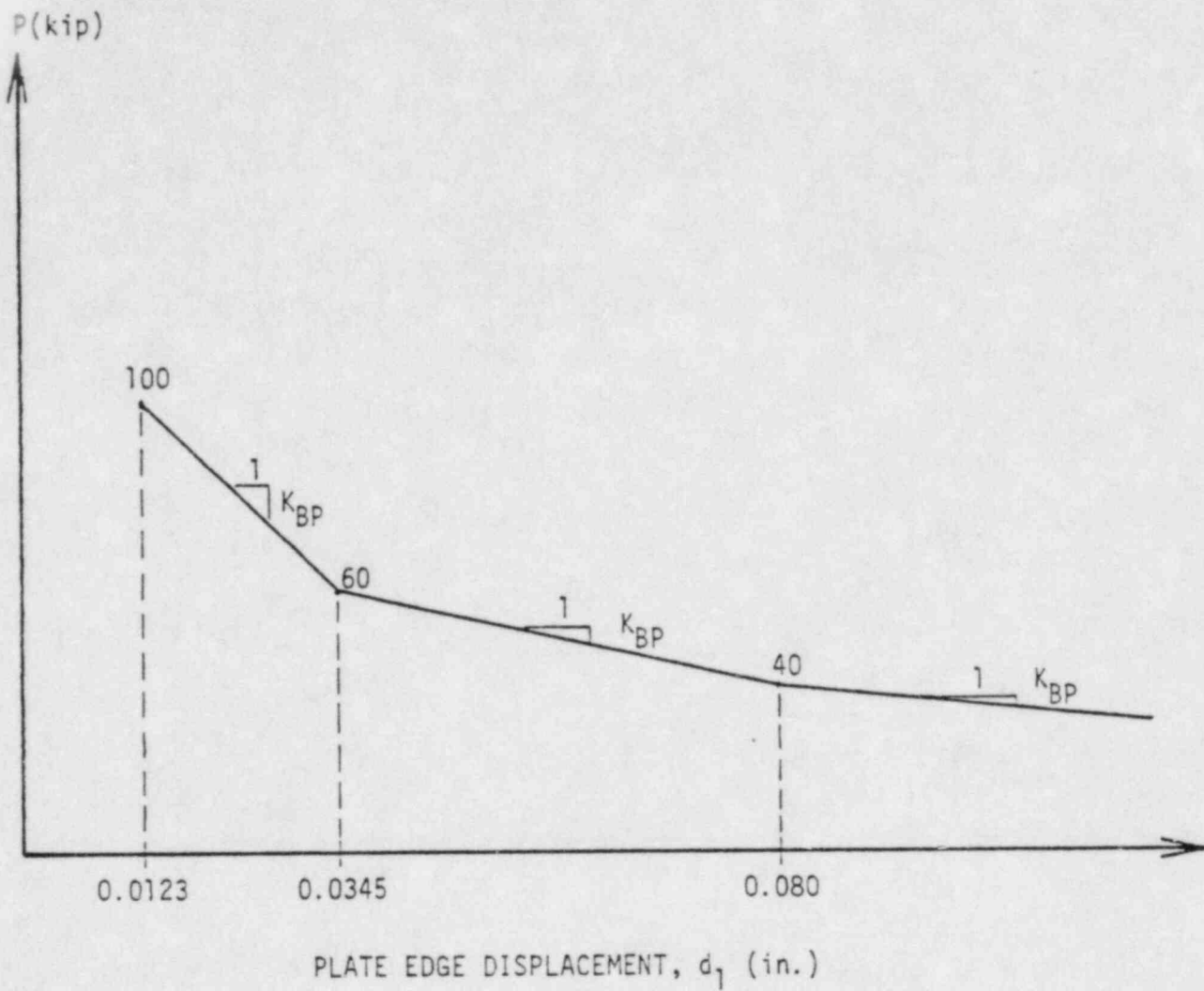


Figure 20. In-plane stiffness of bent plate, K_{BP} in the post-yield condition.

An analysis was not necessary for the load combination without the thermal load because, by inspection, the liner plate would then be subjected to a tensile membrane load.

The analysis results were compared with the applicable design allowables specified in Division 2 of ASME Boiler & Pressure Vessel Code, Section III, Subsection CC-3700. Table 7 shows this comparison. For the liner plate, the maximum strain was compared. For the studs, they were evaluated against the allowable shear force for the load combination without thermal load (i.e., mechanical loads only) and against the allowable displacement for the load combination with thermal load. It can be seen that, except for Case 2, the liner system possesses sufficient capacity when compared with the applicable ASME code design allowables. For the bent-plate case, the maximum anchor displacement exceeded the ASME code allowable by about 10% but still is well within the ultimate capacity. Since we are evaluating an existing liner system rather than designing a new one, we conclude that the liner system is acceptable for the postulated load combination of SSE, LOCA, and other applicable loads.

Table 4. Forces and moments in concrete shell.

	Insulated Zone				Uninsulated Zone			
	D	E	P	D+E+P*	D	E	P	D+E+P*
f_z (k/in.)	-8.2	+ 8.3	16.0	- 0.5	- 7.5	+ 7.9	15.9	0.5
M_z (k-in./in.)	0.	+14.5	97.1	82.6	-11.0	+ 3.6	-78.8	-93.4
f_h (k/in.)	-0.5	+ 1.1	8.5	6.9	0.	+ 0.8	20.1	19.3
M_h (k-in./in.)	0.	+ 3.5	16.5	13.0	0.	+ 3.5	-13.4	-16.9

*The negative forces and moments due to E are used in the load combination to maximize compression (or minimize tension).

Table 5. Liner membrane strains.

Loads	Insulated Zone				Uninsulated Zone			
	s_z (psi)	s_h (psi)	e_z (μ)	e_h (μ)	s_z (psi)	s_h (psi)	e_z (μ)	e_h (μ)
D+E+P	161	154	45	42	-183	322	-238	353
Shrinkage, S	N/A	N/A	-100	-100	N/A	N/A	-100	-100
Thermal, T	N/A	N/A	-263	-263	N/A	N/A	-1335	-1,336
-----			-----	-----			-----	-----
D+E+P+S+T			-318	-321			-1,674	-1,083
D+E+P+S (mechanical loads)			- 55	- 58			- 338	- 253

Table 6. Liner membrane force and unbalanced force in Case 1 analysis model.

	<u>D+E+P+S+T</u>	<u>D+E+P+S</u>
N_z (Insulated Liner) (kip)	- 82	-15
N_z (Uninsulated Liner) (kip)	-204 (-420)*	-55
ΔN_z (kip)	-122	-40

*-204 kip replaces the computed value of -420 kip because the latter exceeds the former, which is the yield load in the plate.

Table 7. Summary of analysis results and ASME allowables.

		Case I		Case II
		<u>D+E+P+S+T</u>	<u>D+E+P+S</u>	<u>D+E+P+S+T</u>
Liner	e_{max}	-1,674 μ	-338 μ	-1,083 μ
Plate	$e_{allowable}$	-5,000 μ	-5,000 μ	-5,000 μ
Liner	d_{max}	0.045 in.	0.012 in.	0.091 in.
Anchor	$d_{allowable}$ ($= \frac{d_u}{2}$)	0.083 in.	N/A	0.083 in.
	V_{max}	10.8 kip	4.7 kip	12.8 kip
	$V_{allowable}$ ($=V_u/2$)	N/A	7.2 kip	N/A

4. SUMMARY AND CONCLUSION

4.1 CONCRETE SHELL STRUCTURE

The reinforced concrete containment structure of the Connecticut Yankee Nuclear Generating Plant was analyzed for these combined load conditions: An SSE using site-specific ground response spectra with peak ground acceleration of 0.21 g in the horizontal direction and 0.14 g in the vertical direction, pressure (peak pressure of 39.3 psig) and thermal transient (peak temperature of 267°F) loads of a LOCA, and the dead weight of the structure.

The containment structure was modeled as an axisymmetrical linear elastic finite-element system composed of conical shell elements. The stiffness effects of the liner system was neglected in determining the structural stiffness. Thermal transient analyses were performed to determine the temperature gradients through the containment structure wall. Equivalent linear gradients were then applied to the shell elements of the finite-element model for the thermal-load case. From the finite element model, section forces and moments through the thickness of the structure wall were obtained. Separate cracked-section analyses were carried out for selected sections, using the section forces and moments obtained from the linear finite-element model, to calculate the stresses in concrete and rebars.

The results of the cracked-section analyses showed that during the LOCA, significant cracks would develop through the thickness of the wall for most part of the structure. The stresses of rebars in hoop and meridian directions at many locations would reach a level just below the yield stress. The maximum predicted radial and tangential shear stresses

in the reinforced concrete shell near the base exceed those allowed by Standard Review Plan and ASME Boiler and Pressure Vessel Code, Section III, Division 2, Subsection CC, under the combined loading conditions of SSE and LOCA.

4.2 LINER-PLATE SYSTEM

The liner-plate system was evaluated for the abnormal/extreme environmental condition which included the SSE and the LOCA pressure and temperature loads. The liner on the cylinder near the upper edge of the insulation, about 20 ft above the base, was analyzed because it is the most critically loaded location. The maximum liner strains, and maximum anchor displacements and loads were computed and evaluated against the allowables specified in ASME Code Section III, Division 2, Subsection CC-3700. The comparison indicated that the anchors in the existing design of the liner-plate system most likely will deform in excess of the code design limit, but still well within the ultimate capacity, when subjected to the combination of SSE and LOCA loads. For the liner plate strains and anchor loads, they will be within the applicable code design allowables. In light of the fact that we are evaluating an existing design and that the analysis method adopted here ignored the biaxial stiffness of the liner system, we conclude the liner system would perform satisfactorily for the postulated load combination.

APPENDIX A. DERIVATION OF FLAT-PLATE STIFFNESS K_{FP}

For the one-dimensional analysis under consideration, the stiffness of the flat plate is determined from the configuration shown in Figure A.1 in which a concentrated load, P , is applied to the plate at every stud anchor. The concentrated load may be assumed to act through a circular area having a diameter D equal to the stud diameter plus the plate thickness. That is, $D = 1/2 \text{ in.} + 3/8 \text{ in.} = 7/8 \text{ in.}$

Because the rigorous solution for the problem shown in Figure A.1 is not readily available, we will assume that the deflection of the anchor point, y , can be approximated by the average of two other solutions, y_a and y_b . y_a is the deflection of the anchor point where a force P is applied to a semi-infinite plate (Figure A.2(a)), but only the stress field within a distance of L from the anchor point is considered. y_b is the deflection of a strip of the plate (Figure A.2(b)) where a uniformly distributed load having a total magnitude of P is applied to one edge of the plate.

For y_a , the radial stress along the y -axis is, according to Reference 7,

$$s_r(\theta = 90^\circ) = 2P/\pi yt \quad (t = \text{plate thickness}) \quad (\text{A-1})$$

Let us define

$$y_a = \frac{(1-0.3^2)}{E_s} \int_0^L \frac{s_r}{D/2} dy \quad (\text{A-2})$$

in which 0.3 and E_s ($= 30,000 \text{ ksi}$) are the Poisson's ratio and Young's modulus of the liner, and $L = 17 \text{ in.}$ Substituting Eq. (A-1) into (A-2) gives

$$y_a = 195 \times 10^{-6} P$$

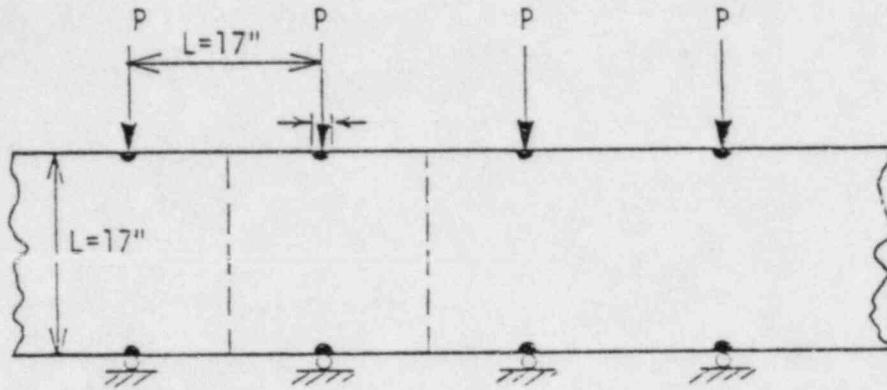


Figure A.1. Model for determining in-plane stiffness K_{Fp} for a flat plate.

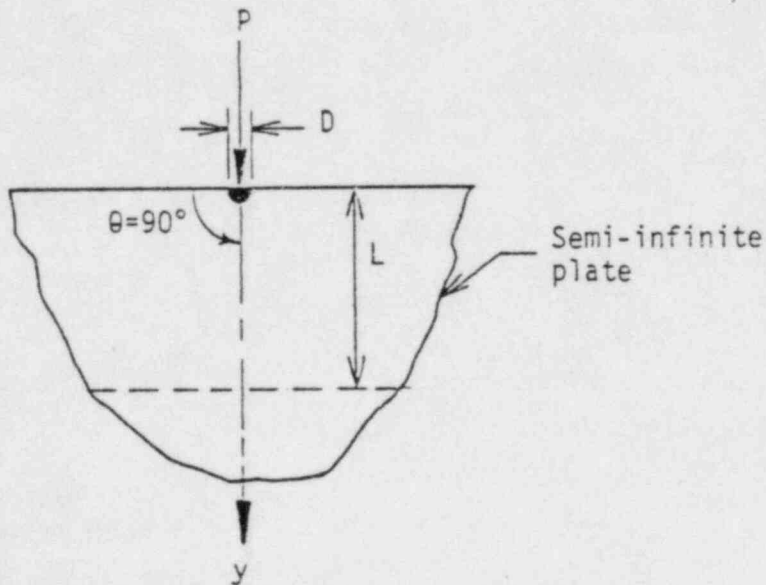


Figure A.2. Approximate analysis model for determining deflection y_a .

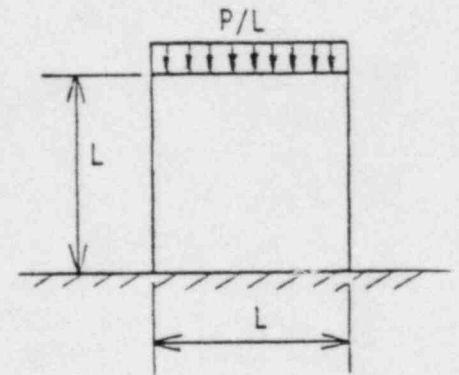


Figure A.3. Analysis model for determining deflection y_b .

For y_b , we have

$$y_b = PL/ELt = 92 \times 10^{-6}P$$

Thus,

$$y \cong (y_a + y_b)/2 = 143 \times 10^{-6}P$$

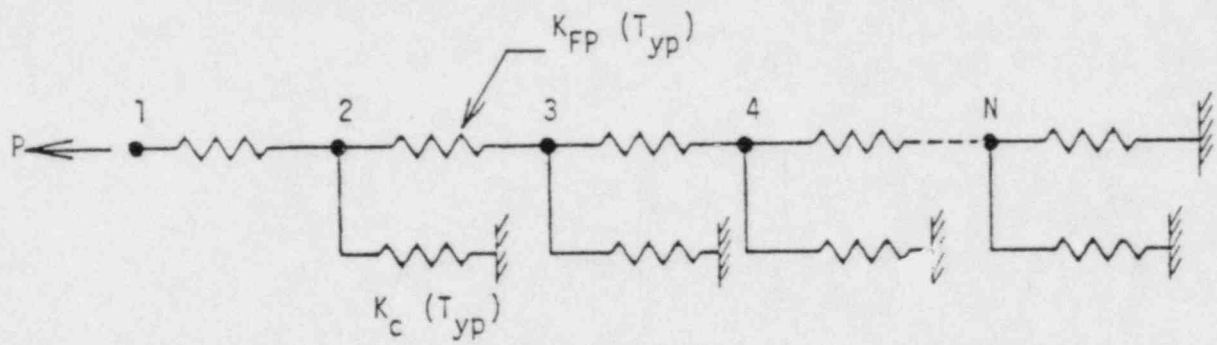
and the approximate in-plane stiffness is

$$K_{FP} = P/y = 6970 \text{ k/in.}$$

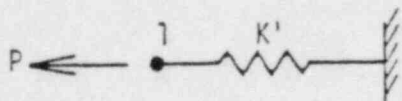
The stiffness is linear until the yield load of the plate, P_y , is reached. For a yield stress of 32 ksi, $P_y = 32 \times 17 \times 3/8 = 204$ kip. The elastic-plastic function for K_{FP} is illustrated in Figure 17 in the text.

Again, $[K_{N-3}]$ is exactly like $[K_{N-2}]$, but another order smaller. Letting

$$\frac{|K_{N-2}|}{|K_{N-1}|} = \frac{|K_{N-3}|}{|K_{N-2}|} = \dots = \frac{|K_{N-i}|}{|K_{N-i+1}|} = \dots = R \quad (B-5)$$



(a) Liner Spring Series



(b) Equivalent Spring.

Figure B.1. Equivalent spring for spring series.

we have, upon using Eq. (B-4),

$$R = \frac{|K_{N-2}|}{|K_{N-1}|} = \frac{|K_{N-2}|}{(2K_{FP} + K_C)|K_{N-2}| - K_{FP}^2|K_{N-3}|} = \frac{1}{(2K_{FP} + K_C)|K_{N-2}| - RK_{FP}^2}$$

Solving for R, we have

$$R = (1+q - \sqrt{(1+q)^2 - 1})/K_{FP} \quad (B-6)$$

$$q = K_C/2K_{FP}$$

Eq. (B-3) then becomes

$$|K_N| = K_{FP} (\sqrt{(1+q)^2 - 1} - q) |K_{N-1}| \quad (B-7)$$

and it can be shown that

$$u_1 = P |K_{N-1}| / |K_N|$$

$$= P/K'$$

where

$$K' = K_{FP} (\sqrt{(1+q)^2 - 1} - q) \quad (B-8)$$

The single-spring equivalent system is illustrated in Figure B.1(b).

APPENDIX C. DERIVATION OF POST YIELD IN-PLANE STIFFNESS,
 K_{BP} , OF A BENT PLATE.

In Figure C.1, the bent plate has an initial transverse deflection Δ_m . According to Reference 8, the transverse deflection at the center of the plate when subjected to an axial load, P, is

$$\Delta = \Delta_m / (1 - P/P_{cr}) \quad C-1$$

where

P_{cr} = Euler's buckling load for a fixed-end beam

$$= \left(\frac{2\pi}{L}\right)^2 \frac{E_s L t^3}{12} = 296 \text{ kip}$$

Normally, flexural yielding takes place prior to buckling. The force required to produce flexural yielding of the plate is related to the transverse displacement of the bent plate as follows:

$$\Delta = \frac{2M_y}{P} \quad (C-2)$$

in which

M_y = yield moment

$$= 1/4 f_y L t^2 = 1/4 \times 32 \times 17 \times (3/8)^2 = 19.1 \text{ k-in.}$$

Therefore, the P- Δ relation for the bent plate is governed either by Eq. (C-1) or (C-2), whichever requires the smaller value of P to cause a given value of Δ . This is represented by the solid curve in Figure C.2, resulting from the intersection of the two curves representing Eqs. (C-1) and (C-2). At the intersection, it can be shown that

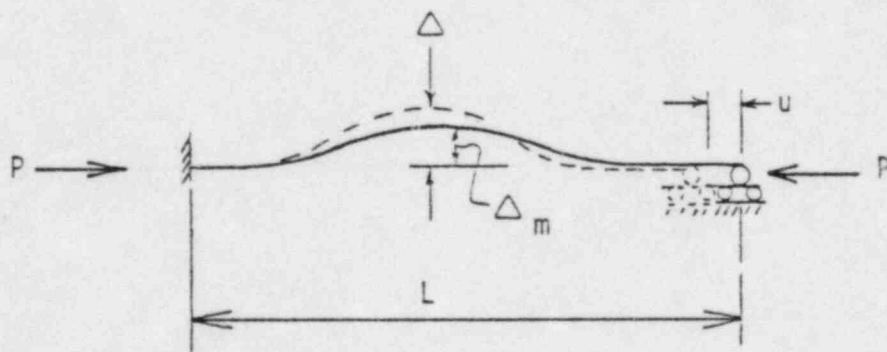


Figure C.1. A bent plate subjected to axial load.

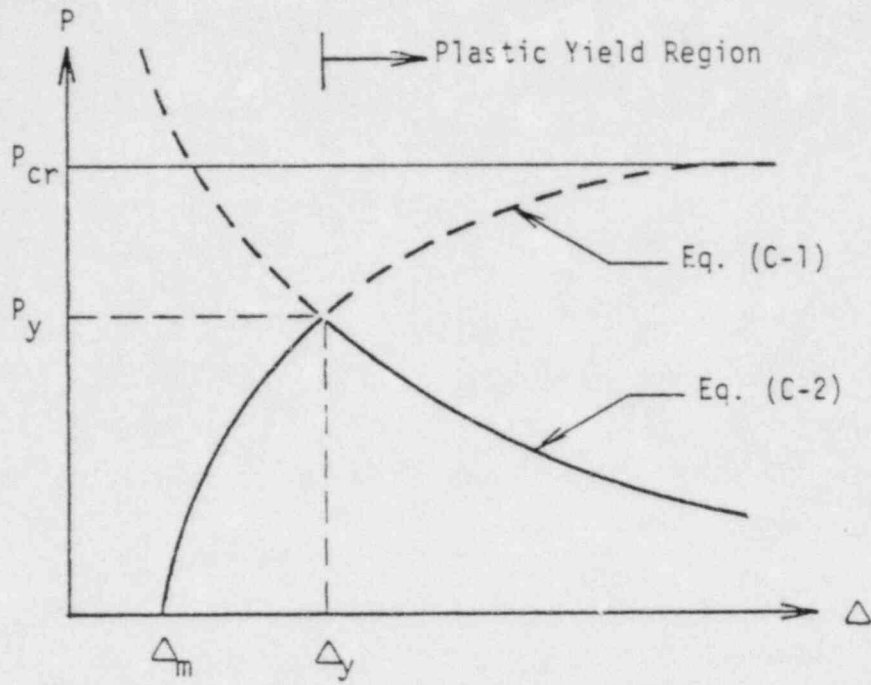


Figure C.2. Force vs transverse deflection relationship for an axially-loaded bent plate.

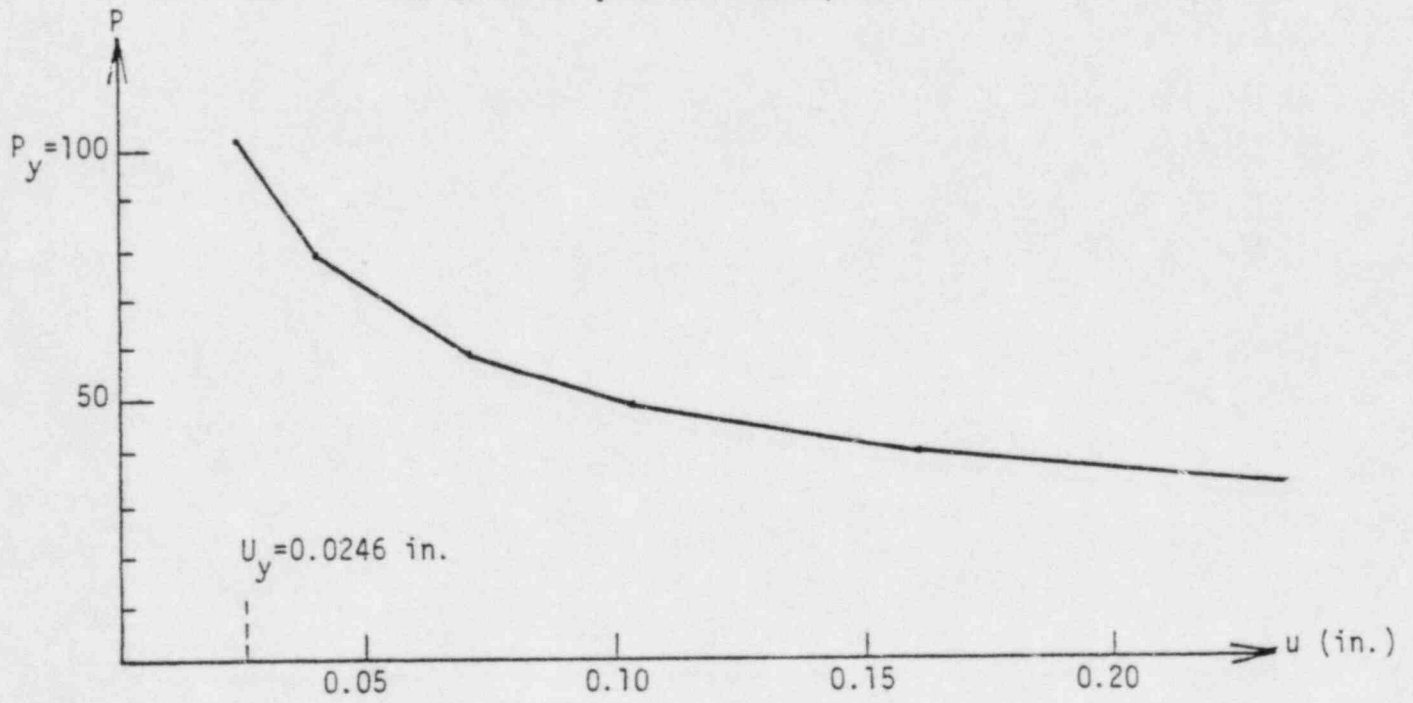


Figure C.3. Force vs axial displacement relationship.

$$P_y = 100 \text{ kip} \tag{C-3}$$

$$\Delta_y = 0.382 \text{ in.}$$

for $\Delta_m = 1/4 \text{ in.}$

We assume that the bent plate has already been stressed into the plastic yielding range so that we only need the in-plane displacement vs force relationship in the plastic region for the liner evaluation. According to References 9, 10, and 11, a semi-empirical formula which correlates reasonably well with test data may be used:

$$u \cong \frac{P}{E_s L t} + \frac{\pi}{a} (\Delta - \Delta_m)^2 \quad \text{for } \Delta > \Delta_y \tag{C-4}$$

$$= \frac{P}{10875} + 0.1848 \left[\left(\frac{38.2^2}{P} \right) - \frac{1}{16} \right]$$

Eq. (C-4) is plotted in Figure C.3. Note that for applications to the liner plate analysis, u is equal to $2d_1$; i.e., twice the displacement of stud No. 1, for analysis Case 2. Thus Figure C.3 is modified to become Figure 20 in the text, to account for the relation between u and d_1 .

REFERENCES

1. Ting-Yu Lo, Lawrence Livermore National Laboratory, letter addressed to S. Brown, SEP, Nuclear Regulatory Commission, May 18, 1982.
2. ANSYS Engineering Analysis System User's Manual, Swanson Analysis Systems, Inc., Houston, Pennsylvania.
3. "Site Specific Ground Response Spectra for SEP Plants located in the Eastern United States" letter of D. M. Crutchfield/NRC to all SEP owners, dated June 8, 1981.
4. Newmark, N.M., Hall, W.P., "Development of Criteria for Seismic Review of Selected Nuclear Power Plants," U.S. NRC, NUREG/CR-0098, May, 1977.
5. C. Y. Liaw, A. Debeling and N. C. Tsai "Structural Review of the Palisades Nuclear Power Plant Unit 1 Containment Structure Under Combined Loads for the Systematic Evaluation Program" Lawrence Livermore National Laboratory, NUREG/CR-2583, UCRL-53033, March, 1982.
6. Design Data, Nelson Concrete Anchor, Studs for Securing Steel to Concrete, Nelson Stud Welding, Div. of Gregory Industries, Inc., Lorain, Ohio, May 1968.
7. Timoshenko and Goodier, Theory of Elasticity, McGraw-Hill Book Co.
8. Timoshenko and Gere, Theory of Elastic Stability, McGraw-Hill, 1961.
9. J. M. Doyle and S. L. Chu, "Liner Plate Buckling and Behavior of Stud and Rib Type Anchors," Second Smirt Conf., Berlin, 1973.
10. Y. I. Moon and T. P. Kicher, "The Plastic Buckling of a Steel Liner Encased in a Concrete Cylinder," Nuclear Eng. and Design, Vol. 41, 1977, p. 281-291.
11. A. G. Young and L. A. Tate, "Design of Liners for Reactor Vessels," Conf. on Prestressed Concrete Pressure Vessels, Inst. Civil Eng., London, Paper J57, 1967.